AGU PUBLICATIONS

Water Resources Research

RESEARCH ARTICLE
10.1002/2013WR014956

Key Points:
- Network reactions are efficiently modeled and fully coupled with particle motion
- Analytical solutions are given for the transport simulation of serial reactions
- Tailing effect due to flow heterogeneity is mitigated in case of decaying solute

Correspondence to:
C. V. Henri,
christopher.henri@upc.edu

Citation:
Henri, C. V., and D. Fernàndez-Garcia (2014), Toward efficiency in heterogeneous multispecies reactive transport modeling: A particle-tracking solution for first-order network reactions, *Water Resour. Res.*, *50*, 7206–7230, doi:10.1002/2013WR014956.

Received 24 OCT 2013
Accepted 18 AUG 2014
Accepted article online 22 AUG 2014
Published online 10 SEP 2014

Toward efficiency in heterogeneous multispecies reactive transport modeling: A particle-tracking solution for first-order network reactions

Christopher V. Henri[1] and Daniel Fernàndez-Garcia[1]

[1]Department of Geotechnical Engineering and Geosciences, Universitat Politècnica de Catalunya, UPC-Barcelona Tech, Barcelona, Spain

Abstract Modeling multispecies reactive transport in natural systems with strong heterogeneities and complex biochemical reactions is a major challenge for assessing groundwater polluted sites with organic and inorganic contaminants. A large variety of these contaminants react according to serial-parallel reaction networks commonly simplified by a combination of first-order kinetic reactions. In this context, a random-walk particle tracking method is presented. This method is capable of efficiently simulating the motion of particles affected by first-order network reactions in three-dimensional systems, which are represented by spatially variable physical and biochemical coefficients described at high resolution. The approach is based on the development of transition probabilities that describe the likelihood that particles belonging to a given species and location at a given time will be transformed into and moved to another species and location afterward. These probabilities are derived from the solution matrix of the spatial moments governing equations. The method is fully coupled with reactions, free of numerical dispersion and overcomes the inherent numerical problems stemming from the incorporation of heterogeneities to reactive transport codes. In doing this, we demonstrate that the motion of particles follows a standard random walk with time-dependent effective retardation and dispersion parameters that depend on the initial and final chemical state of the particle. The behavior of effective parameters develops as a result of differential retardation effects among species. Moreover, explicit analytic solutions of the transition probability matrix and related particle motions are provided for serial reactions. An example of the effect of heterogeneity on the dechlorination of organic solvents in a three-dimensional random porous media shows that the power-law behavior typically observed in conservative tracers breakthrough curves can be largely compromised by the effect of biochemical reactions.

1. Introduction

Monitored natural attenuation is a cheap and environmentally respectful cleanup tool for organic and inorganic contaminants in groundwater [*MacDonald*, 2000]. As advised by the United State Environmental Protection Agency this approach should always be firstly considered by groundwater managers in his decision-making process [*United States Environmental Protection Agency*, 1998]. Yet the inherent complexity of a natural system typically challenges the assessment of these type of technologies [*Soga et al*., 2004; *Bolster et al*., 2009]. The spatial variability of aquifer properties and the contaminant biochemical conditions complicate the analysis of a groundwater polluted site. Thus, the hydraulic conductivity can vary several orders of magnitude even in relatively mild heterogeneous aquifers [*Gelhar*, 1993; *Rubin*, 2003]. This typically leads to geological structures with preferential channels [*Sanchez-Vila et al*., 1996; *Gomez-Hernandez and Wen*, 1998; *Trinchero et al*., 2008] and low permeability areas where contaminants can be trapped and slowly released in time [*Stroo et al*., 2012; *de Barros et al*., 2013]. Moreover, degradation rates of contaminants in aquifers can vary substantially in space [*Allen-King et al*., 2006] due to, for instance, changes in the bacteria activity responsible for biodegradation [e.g., *Fennell et al*., 2001; *Sandrin et al*., 2004]. The effect of these different types of heterogeneities should not be considered independently. The joint effect and correlation of the processes underlying these different sources of variability can be equally important to assess the fate and transport of contaminants [*Rehfeldt et al*., 1992; *Cunningham and Fadel*, 2007].

In addition, the evolution of many contaminants in natural systems results from network reactions given by sets of chemical species that react simultaneously to produce different species. For example, hazardous

waste sites contaminated with chlorinated solvents such as tetrachloroethylene (PCE) and trichloroethylene (TCE) involve a serial reaction pathway resulting from anaerobic reductive dechlorination [*McCarty and Semprini*, 1994]. In such a case, PCE will be transformed into TCE, and TCE will be biodegraded into DCE (dichloroethylene). Subsequently, DCE will react to produce vinyl chloride (VC) [*Skeen et al*., 1995; *Jain and Criddle*, 1995]. The toxicity of each of these species is different and, consequently, the analysis of the risk posed by these contaminants to human health is a complicated process [*Benekos et al*., 2006]. In this context, it is clear that an adequate analysis of natural attenuation requires efficient numerical methods capable of incorporating complex network reactions with spatially varying hydrobiochemical properties.

Even though model predictions can be strongly affected by the spatial variability of both hydraulic and biochemical properties [*Rehfeldt et al*., 1992; *Miralles-Wilhelm and Gelhar*, 1996; *Miralles-Wilhelm et al*., 1997; *Cunningham and Fadel*, 2007; *Maxwell and Kastenberg*, 1999; *Maxwell et al*., 2007], reactive transport codes based on Eulerian methods such as finite-difference or finite elements [e.g., *Saaltink et al*., 2004; *Clement*, 1997] still undergo computational burden and numerical problems when modeling strong heterogeneities and complex biochemical systems at high resolution. In this context, Particle Tracking Methods (PTMs) offer a convenient numerical solution particularly efficient in dealing with heterogeneities [e.g., *Wen and Gómez-Hernández*, 1996; *LaBolle et al*., 1996; *Salamon et al*., 2007; *Riva et al*., 2008] and a large variety of complex transport processes such as non-Fickian transport [*Delay and Bodin*, 2001; *Cvetkovic and Haggerty*, 2002; *Berkowitz et al*., 2006; *Zhang and Benson*, 2008; *Dentz and Castro*, 2009] and multiple porosity systems [*Salamon et al*., 2006b; *Benson and Meerschaert*, 2009; *Tsang and Tsang*, 2001; *Huang et al*., 2003; *Willmann et al*., 2013]. Moreover, this methodology, which is always mass conservative, avoids some of the inherent numerical difficulties associated with Eulerian approaches, i.e., numerical dispersion and oscillations due to truncation errors [*Salamon et al*., 2007; *Boso et al*., 2013].

Several disadvantages have prevented the general use of PTMs in reactive transport problems. One of the main problems is that the reconstruction of concentrations from a limited number of particles can develop spurious fluctuations [*Kinzelbach*, 1987; *Bagtzoglou et al*., 1992; *Salamon et al*., 2006a; *Boso et al*., 2013]. Even though these problems can be largely minimized by using optimal kernel density estimation methods [*Fernàndez-Garcia and Sanchez-Vila*, 2011; *Pedretti and Fernàndez-Garcia*, 2013b], PTMs are more efficient when the computation of solute concentrations is not necessary during the course of the simulation. This implies that the statistical fluctuations associated to the calculation of concentrations at one time step cannot propagate as the computations are continued. However, this also means that concentration dependent chemical processes are not easily incorporated into PTMs without a significant trade-off with respect to computational efficiency and accuracy [e.g., *Tompson*, 1993; *Tompson et al*., 1996; *Cui et al*., 2014].

Some chemical reactions can be efficiently incorporated into PTMs without having to recalculate concentrations at each time step. For instance, first-order degradation reactions of a single species can be included into PTMs by assigning to every particle a variable mass, which develops in time according to first-order kinetics [*Kinzelbach*, 1987; *Wen and Gómez-Hernández*, 1996]. When all species share the same transport operator, certain reactions in chemical equilibrium can be easily simulated with particle tracking by using conservative components [*Molins et al*., 2004; *Kräutle and Knabner*, 2005; *De Simoni et al*., 2005; *Fernàndez-Garcia et al*., 2008; *Fernàndez-Garcia and Sanchez-Vila*, 2011], i.e., a linear combination of the species concentrations that can be used to decouple the system of equations into simpler problems. Fast kinetic reactions have been properly simulated by applying simple proximity relationships between nearby particles [*Edery et al*., 2009, 2010]. Rate-limited kinetic chemical reactions in a well-stirred batch system can be simulated by using the Gillespie algorithm [*Gillespie*, 1976]. This method can be used to model geochemical reactions in porous media [*Palanichamy et al*., 2007]. However, its application to reactive transport suffers from having to define the scale at which sufficient mixing occurs (the representative volume of a particle). To overcome this, encounter probability distribution functions have been derived to simulate simple bimolecular kinetic reactions [*Benson and Meerschaert*, 2008; *Paster et al*., 2014]. Modeling transport with other types of nonlinear complex chemical reactions based only on particles is still a challenge nowadays.

Several algorithms have also been introduced to simulate kinetic sorption of a single species. Some of them are based on transition probabilities [*Kinzelbach*, 1987; *Andričević and Foufoula-Georgiou*, 1991; *Michalak and Kitanidis*, 2000] and others on the probability distribution of the particle residence time in the liquid and solid phase [*Valocchi and Quinodoz*, 1989; *Painter et al*., 2008]. In general, the efficiency of these methods depends on the parameters adopted to simulate transport. Nevertheless, it is worth mentioning that

Michalak and Kitanidis [2000] found that their semianalytical moment method was as accurate as others but significantly more computationally efficient for a wide range of parameter values. This method is limited to kinetically sorbing solutes and locally homogeneous media with constant velocity.

This paper proposes an efficient method to simulate complex network reactions in heterogeneous systems using a random walk particle tracking approach. The approach is limited to first-order kinetic reactions which is a common simplification of many reaction networks. Even though it is desirable to model microbial biotransformation rates through Monod or Michaelis-Menten enzyme kinetics, the concentration of dissolved organics in many contaminated sites is less than that of the Michaelis half-saturation constant. In this situation, it is often convenient to express transformation rates by pseudofirst-order reaction rates [e.g., *Bouwer et al*., 1981; *Vogel et al*., 1987; *Haston and McCarty*, 1999; *Burnell et al*., 2014]. Nuclear waste sites contaminated with radioactive species, pesticides, organic phosphates, and nitrogen species transformations have been also typically modeled through first-order network reactions [e.g., *van Genuchten*, 1985; *Mishra and Mishra*, 1991; *Vishwanathan et al*., 1998].

Among other results, the paper shows the effect of biochemical network reactions on the motion and chemical state of particles, which is determined from the solution matrices of the spatial moments governing equations. The method extends the concept of transition probabilities [e.g., *Michalak and Kitanidis*, 2000; *Salamon et al*., 2006a, 2006b] to first-order reaction networks and develops analytical solutions of the transition matrices associated with serial reactions.

The paper is organized as follows: Firstly, the mathematical framework leading to the calculation of transition probabilities and related equations of particle motion is developed. This is then incorporated into a random walk particle model. At this point, the validation and justification of the new particle tracking algorithm is presented. Finally, the capabilities of the new method are illustrated by simulating the reductive dechlorination of PCE in a three-dimensional spatially heterogeneous system.

2. Governing Equations

2.1. Transport Equations of Network Reactions

The transport equations governing the behavior of network reactions may be written for diluted chemical systems as a set of advective-dispersive equations coupled with first-order reactions [e.g., *Clement*, 1997, 2001; *Sun et al*., 1999]

$$\phi R_i \frac{\partial c_i}{\partial t} - \nabla \cdot (\phi \mathbf{D} \nabla c_i) + \nabla \cdot (\mathbf{q} c_i) = \sum_{j=1}^{n_s} y_{ij} k_j \phi c_j, \quad \forall i = 1, \ldots, n_s, \tag{1}$$

where the ith-equation represents the mass balance of the ith species, n_s is the number of the species involved, ϕ is the porosity of the media, $\mathbf{q}$ [L T^{-1}] is the Darcy velocity vector, and $\mathbf{D}$ [L^2 T^{-1}] is the dispersion tensor. For any given species i, R_i (dimensionless) is the retardation factor, c_i [M L^{-3}] is the concentration in the liquid phase, k_i [T^{-1}] is the first-order contaminant destruction rate constant, and y_{ij} [M M^{-1}] is the effective yield coefficient for any reactant or product pair. These coefficients are defined as the ratio of mass of species i generated to the amount of mass of species j consumed.

Sorption reactions are assumed to be in local equilibrium and to follow a linear sorption isotherm. For mathematical convenience, here the notation considers that the yield coefficients y_{ii} ($j = i$) are equal to -1, which represents the biodecay of the ith species. Also, it has been assumed that, without loss of generality, only aqueous concentrations are subject to chemical reactions, i.e., no biodegradation in the sorbed phase occurs. Other scenarios can be simulated by properly redefining the degradation rates [*van Genuchten*, 1985]. Note that all properties are defined as spatially varying coefficients.

2.2. Spatial Moments Differential Equations

In particle tracking methods the evolution of a solute plume is approximated by a discrete number of moving particles. The spatial position and attributes of each particle are then changed in time according to simple relationships. In this work these fundamental relationships are derived so as to satisfy (2). For this, we will consider the approach of *Kitanidis* [1994] and *Salamon et al*. [2006b], which assume that each particle

can be seen as a small plume that moves according to its spatial moments. The governing equations of the spatial moments of a network reaction system can be derived as follows.

Let us start by expressing the system of transport equations in terms of total densities ρ_i, defined as the sum of aqueous mass and sorbed mass of a given species i per unit volume, i.e., $\rho_i = \phi R_i c_i$. Thus,

$$\frac{\partial \rho_i}{\partial t} - \nabla \cdot \left(\phi \mathbf{D} \nabla \frac{\rho_i}{\phi R_i} \right) + \nabla \cdot \left(\mathbf{q} \frac{\rho_i}{\phi R_i} \right) = \sum_{j=1}^{n_s} K_{ij} \rho_j, \quad \forall i = 1, \ldots, n_s, \tag{2}$$

where $K_{ij} = y_{ij} k_j / R_j$. The first three absolute spatial moments of a solute plume are defined as

$$m_i^0(t) = \int \rho_i(\mathbf{x}, t) dV, \quad \forall i = 1, 2, \ldots, n_s, \tag{3}$$

$$\mathbf{m}_i^1(t) = \int \mathbf{x} \rho_i(\mathbf{x}, t) dV, \quad \forall i = 1, 2, \ldots, n_s, \tag{4}$$

$$\mathbf{m}_i^2(t) = \int \mathbf{x} \cdot \mathbf{x}^t \rho_i(\mathbf{x}, t) dV, \quad \forall i = 1, 2, \ldots, n_s. \tag{5}$$

The zeroth spatial moment m_i^0 is the total mass of the ith species. Its temporal evolution will help determining the chemical state (species) assigned to a given particle at a later time. The first and second spatial moments, $\mathbf{m}_i^1$ and $\mathbf{m}_i^2$, describe the position of the center of mass of species i and its spread about the origin of coordinates, respectively. They will be used to move particles by advection and dispersion.

Since a particle located at position $\mathbf{x}_t$ and time t can be seen as an infinitely small plume [*Kitanidis*, 1994], its total density and related moments can be represented by

$$\rho_i(\mathbf{x}, t) = m_i^0 \delta(\mathbf{x} - \mathbf{x}_t), \quad \forall i = 1, 2, \ldots, n_s, \tag{6}$$

$$\mathbf{x} \rho_i(\mathbf{x}, t) = \mathbf{m}_i^1 \delta(\mathbf{x} - \mathbf{x}_t), \quad \forall i = 1, 2, \ldots, n_s, \tag{7}$$

$$\mathbf{x} \cdot \mathbf{x}^t \rho_i(\mathbf{x}, t) = \mathbf{m}_i^2 \delta(\mathbf{x} - \mathbf{x}_t), \quad \forall i = 1, 2, \ldots, n_s. \tag{8}$$

where the Dirac function δ expresses the strict consideration of the plume system as a particle. Accepting that mass fluxes far away from the particle plume are negligible and following the procedure described by *Kitanidis* [1988], integration by parts of (2) considering (6)–(8) yields

$$\frac{dm_i^0}{dt} = \sum_{j=1}^{n_s} K_{ij} m_j^0, \quad \forall i = 1, 2, \ldots, n_s, \tag{9}$$

$$\frac{d\mathbf{m}_i^1}{dt} = \frac{\mathbf{q}_p}{\phi R_i} m_i^0 + \sum_{j=1}^{n_s} K_{ij} \mathbf{m}_j^1, \quad \forall i = 1, 2, \ldots, n_s, \tag{10}$$

$$\frac{d\mathbf{m}_i^2}{dt} = (\mathbf{m}_i^1) \cdot \frac{\mathbf{q}_p^t}{\phi R_i} + \frac{\mathbf{q}_p}{\phi R_i} \cdot (\mathbf{m}_i^1)^t + \frac{2\mathbf{D}}{R_i} m_i^0 + \sum_{j=1}^{n_s} K_{ij} \mathbf{m}_j^2, \quad \forall i = 1, 2, \ldots, n_s, \tag{11}$$

where $\mathbf{q}_p$ is the modified darcy velocity, defined as $\mathbf{q}_p = \mathbf{q} + \nabla \cdot (\phi \mathbf{D})$. The components of this vector are expressed as $\mathbf{q}_p = (q_x', q_y', q_z')^t$ from then on. Moreover, all parameters will be considered at the particle position $\mathbf{x}_t$. For the sake of notational simplicity this dependence will be shown only when its omission might create confusion.

Equations (9)–(11) constitute a linear system of ordinary differential equations (ODE) that can be solved sequentially. The first equation (9) describes the mass transformation due to biochemical reactions. The other two equations, (10) and (11), describe the advective-dispersive motion of a particle. The first terms on the left hand-side of these equations is the standard random walk motion of a particle [*Kinzelbach*, 1987; *Tompson and Gelhar*, 1990; *Salamon et al.*, 2006a]. Interestingly, the last term is an additional quantity that takes into consideration the fact that the motion of a particle is also affected by biochemical reactions. The importance of this term will be explored in section 6.1.

In order to solve this ODE system it is convenient to analyze each component of the vector $\mathbf{m}_i^1$ and the matrix $\mathbf{m}_i^2$ independently. Let us consider for instance the component x of $\mathbf{m}_i^1$ and the component xy of $\mathbf{m}_i^2$ and define the following vectors

$$\boldsymbol{\mu}=(m^0_1,\ldots,m^0_{n_s})^t,$$
$$\boldsymbol{\chi}_x=(m^1_{1,x},\ldots,m^1_{n_s,x})^t,$$
$$\boldsymbol{\psi}_{xy}=(m^2_{1,xy},\ldots,m^2_{n_s,xy})^t.$$

The system of equations can then be rewritten as

$$\frac{d\boldsymbol{\mu}}{dt}=\mathbf{K}\boldsymbol{\mu}, \tag{12}$$
$$\frac{d\boldsymbol{\chi}_x}{dt}=\frac{q'_x}{\phi}\mathbf{R}^{-1}\boldsymbol{\mu}+\mathbf{K}\boldsymbol{\chi}_x, \tag{13}$$
$$\frac{d\boldsymbol{\psi}_{xy}}{dt}=\frac{q'_y}{\phi}\mathbf{R}^{-1}\boldsymbol{\chi}_x+\frac{q'_x}{\phi}\mathbf{R}^{-1}\boldsymbol{\chi}_y+2D_{xy}\mathbf{R}^{-1}\boldsymbol{\mu}+\mathbf{K}\boldsymbol{\psi}_{xy}, \tag{14}$$

where $\mathbf{R}$ is a diagonal matrix composed of retardation factors, i.e., $\mathbf{R}=\mathrm{diag}\{R_1,\ldots,R_{n_s}\}$. The theory of linear differential equations assures that n_s linearly independent solutions for systems (12), (13) and (14) always exist, which may be labeled as

$$\boldsymbol{\mu}^{(1)}(t),\ldots,\boldsymbol{\mu}^{(n_s)}(t),$$
$$\boldsymbol{\chi}_x^{(1)}(t),\ldots,\boldsymbol{\chi}_x^{(n_s)}(t),$$
$$\boldsymbol{\psi}_{xy}^{(1)}(t),\ldots,\boldsymbol{\psi}_{xy}^{(n_s)}(t).$$

Since any solution can be written as a linear combination of these independent solutions, it is often convenient to lump the individual solution vectors together to a so-called *solution matrix*. We define thereby the solution matrix $\mathbf{M}$, $\mathbf{X}_x$ and $\boldsymbol{\Psi}_{xy}$ as

$$\mathbf{M}=(\boldsymbol{\mu}^{(1)},\ldots,\boldsymbol{\mu}^{(n_s)}),$$
$$\mathbf{X}_x=(\boldsymbol{\chi}_x^{(1)},\ldots,\boldsymbol{\chi}_x^{(n_s)}),$$
$$\boldsymbol{\Psi}_{xy}=(\boldsymbol{\psi}_{xy}^{(1)},\ldots,\boldsymbol{\psi}_{xy}^{(n_s)}),$$

The solution matrix obeys also the following differential system of equations

$$\frac{d\mathbf{M}}{dt}=\mathbf{K}\mathbf{M}, \tag{15}$$
$$\frac{d\mathbf{X}_x}{dt}=\frac{q'_x}{\phi}\mathbf{R}^{-1}\mathbf{M}+\mathbf{K}\mathbf{X}_x, \tag{16}$$
$$\frac{d\boldsymbol{\Psi}_{xy}}{dt}=\frac{q'_y}{\phi}\mathbf{R}^{-1}\mathbf{X}_x+\frac{q'_x}{\phi}\mathbf{R}^{-1}\mathbf{X}_y+2\mathbf{D}_{xy}\mathbf{R}^{-1}\mathbf{M}+\mathbf{K}\boldsymbol{\Psi}_{xy}. \tag{17}$$

This differential system of equations is coupled but can be solved sequentially provided that an initial condition is given. Based on this, the next sections show that the change in the chemical state (species) of a particle and its corresponding motion are dictated by the set of solutions associated to a solute plume of initial mass equal to one, and first and second absolute spatial moments equal to zero. This is mathematically written as

$$\mathbf{M}(t=0)=\mathbf{Id},$$
$$\mathbf{X}_x(t=0)=\mathbf{0},$$
$$\boldsymbol{\Psi}_{xy}(t=0)=\mathbf{0}.$$

The solution matrices associated with other directions will be simply obtained by substituting the subscripts x and y by other coordinate directions $\{x, y, z\}$.

3. Species State Transition Probabilities

Let us consider the zeroth absolute moment. The solution for $\mathbf{M}(t)$ under the initial condition $\mathbf{M}(t=0)=\mathbf{Id}$ is the species state transition probability matrix $\mathbf{P}(t)$. The components $P_{ij}(t)$ of this matrix express the

probability that a given species j at time $t = 0$ will be transformed into another species i at a later time t due to biochemical reactions. This is demonstrated by noticing that the system of equations given by (15) can be seen as the *forward equations* of a continuous-time markov chain process in which the state space is the n_s possible species available in the network reaction system [*Lawler*, 2006]. This approach has been used in chemical physics to model chemical reactions [*Tamir*, 1998; *Kurtz*, 2003].

This can also be explained by physical principles. Consider, for instance, a system that evolves from an initial condition given by $\boldsymbol{\mu}(t=0)=(1,0,\ldots,0)^t$. When all particles have the same mass, the probability $P_{i1}(t)$ that a particle initially being species 1 is transformed into any species i at a later time t can be estimated by the mass fraction of the species $\boldsymbol{\mu}(t)$. Repeating this for any given initial species $j=1,\ldots,n_s$ leads to the transition probability matrix $\mathbf{P}(t)$.

Under heterogeneous biochemical conditions, the solution of (15) is expressed by the *Peano-Baker* series

$$\mathbf{P}(t)=\mathbf{Id}+\int_0^t \mathbf{K}(\mathbf{x}_{\tau_1})d\tau_1+\int_0^t \mathbf{K}(\mathbf{x}_{\tau_1})\int_0^{\tau_1} \mathbf{K}(\mathbf{x}_{\tau_2})d\tau_2 d\tau_1+\ldots. \tag{18}$$

Nevertheless, when a small enough time step is considered, as typically used in particle tracking methods, an approximation of (18) can be given by

$$\mathbf{P}(t)=\exp\left(\mathbf{K}(\mathbf{x}_t)t\right). \tag{19}$$

The only complexity in (19) consists in solving the exponential of a matrix. Different techniques exist to evaluate such a matrix [*Moler and van Loan*, 2003; *Salamon et al*., 2006a, 2006b]. Among them, it is observed that, for particle tracking purposes, a very convenient approach is the diagonalization of a matrix. Since the biochemical properties typically vary among the different species, the matrix $\mathbf{K}$ has distinct eigenvalues and can be therefore decomposed as $\mathbf{K}=\mathbf{S}\mathbf{K}'\mathbf{S}^{-1}$, where $\mathbf{K}'$ is a diagonal matrix formed from the eigenvalues of $\mathbf{K}$, and the columns of $\mathbf{S}$ are the corresponding eigenvectors of $\mathbf{K}$. Based on this, the solution matrix (19) can be written for small time steps as

$$\mathbf{P}(t)=\mathbf{S}(\mathbf{x}_t)\exp\left(\mathbf{K}'(\mathbf{x}_t)t\right)\mathbf{S}^{-1}(\mathbf{x}_t). \tag{20}$$

The eigensystem of a matrix can be determined by several numerical methods [*Smith et al*., 1976]. Nevertheless, as shown in section 6.1, simple analytical solutions can be obtained for important particular cases, e.g., serial reactions.

4. First and Second Spatial Moments

Having solved the mass evolution of a particle, we can now determine the first and second spatial moments. It is important here to focus on the normalized first spatial moment $\mathbf{A}_{ij}$ and the normalized second central spatial moment $\mathbf{B}_{ij}$ defined as

$$\mathbf{A}_{ij}(t)=\frac{1}{P_{ij}(t)}\left(X_{x,ij}(t),X_{y,ij}(t),X_{z,ij}(t)\right)^t, \tag{21}$$

$$\mathbf{B}_{ij}(t)=\mathbf{B}'_{ij}(t)-\mathbf{A}_{ij}(t)\mathbf{A}^t_{ij}(t), \tag{22}$$

where

$$\mathbf{B}'_{ij}(t)=\frac{1}{P_{ij}(t)}\begin{pmatrix}\Psi_{xx,ij}(t) & \Psi_{xy,ij}(t) & \Psi_{xz,ij}(t)\\ \Psi_{yx,ij}(t) & \Psi_{yy,ij}(t) & \Psi_{yz,ij}(t)\\ \Psi_{zx,ij}(t) & \Psi_{zy,ij}(t) & \Psi_{zz,ij}(t)\end{pmatrix}. \tag{23}$$

Suppose that the particle plume initially associated with species j is transformed into species i in a given time interval t, the matrix $\mathbf{A}_{ij}(t)$ and $\mathbf{B}_{ij}(t)$ describe, respectively, the position of the center of mass of the particle plume and the spread about its center. An outline of the derivation of the spatial moments is provided in Appendices A and B. The solution can be written in terms of effective parameters as

$$\mathbf{A}_{ij}(t)=\frac{\mathbf{q}_p t}{\phi R^e_{ij}(t)}, \tag{24}$$

$$\mathbf{B}_{ij}(t)=\frac{2\mathbf{D}^e_{ij}(t)}{R^e_{ij}(t)}t, \tag{25}$$

where R^e_{ij} is the effective retardation factor and $\mathbf{D}^e_{ij}$ is the effective dispersion coefficient given by

$$R^e_{ij}(t)=P_{ij}(t)\left(\sum_{p,q,r=1}^{n_s} S_{ip}S^{-1}_{pq}R^{-1}_{qq}S_{qr}S^{-1}_{rj}F_{pr}(t)\right)^{-1}, \tag{26}$$

$$\mathbf{D}^e_{ij}=\mathbf{D}+\left(\frac{R^e_{ij}(t)}{G_{ij}(t)}-\frac{1}{2R^e_{ij}(t)}\right)\frac{\mathbf{q}_p\mathbf{q}^t_p}{\phi^2}t, \tag{27}$$

where

$$G_{ij}(t)=P_{ij}(t)\left(\sum_{a,b,p,q,r=1}^{n_s}\frac{S_{ia}S^{-1}_{ab}S_{bp}S^{-1}_{pq}S_{qr}S^{-1}_{rj}}{R_{bb}R_{qq}}H_{apr}(t)\right)^{-1}. \tag{28}$$

The matrix function $\mathbf{F}(t)$ and $\mathbf{H}(t)$ are defined in the Appendices A and B, respectively. The temporal behavior of the effective retardation factor and the effective dispersion coefficient will be explored in section 6 for a serial reaction system. Nevertheless, while these expressions are fairly complex, several limiting solutions are worth mentioning. For small times, these matrix functions can be approximated by

$$F_{pr}(t)=\exp\left(\frac{K_{pp}}{2}t\right)\exp\left(\frac{K_{rr}}{2}t\right), \tag{29}$$

$$H_{apr}(t)=\frac{1}{2}\exp\left(\frac{K_{aa}}{3}t\right)\exp\left(\frac{K_{pp}}{3}t\right)\exp\left(\frac{K_{rr}}{3}t\right). \tag{30}$$

Based on this, the effective retardation factor of a particle initially associated with species j and transformed into species i at a later time t can be seen as a simple weighted average of the retardation factors involved in the network reaction system. The weights are given by the transition probability matrix evaluated at the midpoint,

$$R^e_{ij}(t)=P_{ij}(t)\left(\sum_{k=1}^{n_s}P_{ik}(t/2)R^{-1}_{kk}P_{kj}(t/2)\right)^{-1}. \tag{31}$$

Likewise, the matrix function $\mathbf{G}(t)$ can be approximated by

$$G_{ij}(t)=2P_{ij}(t)\left(\sum_{b,q=1}^{n_s}P_{ib}(t/3)R^{-1}_{bb}P_{bq}(t/3)R^{-1}_{qq}P_{qj}(t/3)\right)^{-1}. \tag{32}$$

Interestingly, when all retardation factors have similar values ($R=R_{11}=\ldots=R_{n_sn_s}$), these expressions reduce to

$$R^e_{ij}(t)=R, \tag{33}$$

$$\mathbf{D}^e_{ij}=\mathbf{D}, \tag{34}$$

where, in this case, $G_{ij}(t)=2R^2$ is used. Essentially, this result reflects that even in homogeneous porous media the time dependence of the effective retardation factor and dispersion coefficient can develop as a result of differential retardation factors among species. In a real field setting, this effect will be masked by other phenomena such as the impact of heterogeneity [e.g., *Rajaram and Gelhar*, 1993; *Rajaram*, 1997; *Fernàndez-Garcia et al*., 2005b; *Dentz and Castro*, 2009] or incomplete mixing [e.g., *Sanchez-Vila et al*., 2010; *Dentz et al*., 2011].

5. The Particle Tracking Algorithm

In order to simulate a multispecies reactive transport problem with particle tracking, the distribution of mass of each species were represented by a different cloud of particles. The challenge here is then to define, from initial conditions, the species and position that a given particle will be associated with after a given time t. To do so, each particle is defined by its position $\mathbf{x}_t$ and species state s_t at time t. Knowing the

particle conditions at a given time $[\mathbf{x}_t; s_t]$, we aim then to define the condition in a later time $[\mathbf{x}_{t+dt}; s_{t+dt}]$. The change in chemical state is determined from the species state transition probability matrix $\mathbf{P}(t)$, while the corresponding particle motion is given by the first and second spatial moments. More specifically, the random walk algorithm is as follows.

For each time step dt a random number r is generated from an uniform distribution in a unit interval and the new species state s_{t+dt} is to be that integer μ for which

$$\sum_{i=1}^{\mu-1} P_{ij}(dt) < r \leq \sum_{i=1}^{\mu} P_{ij}(dt). \tag{35}$$

Knowing its species at time t and $t + dt$, a particle will move according to its corresponding spatial moments given by (24) and (25) with $j = s_t$ and $i = s_{t+dt}$. Based on this, the particle will move as

$$\mathbf{x}_{t+dt} = \mathbf{x}_t + \mathbf{A}_{ij}(dt) + \mathbf{B}_{ij}^{1/2}(dt) \cdot \xi(dt), \tag{36}$$

$$\{\mathbf{B}_{ij}^{1/2}\}\{\mathbf{B}_{ij}^{1/2}\}^t = \mathbf{B}_{ij}, \tag{37}$$

where ξ(t) is a normally distributed random variable with zero mean and unit variance, and $\mathbf{x}_t$ is the position of the particle at time t. In the limit, when the number of particles tends to infinity, the particle mass density that evolves from the repeated application of (35) and (36) will satisfy the reactive transport equation (2). Since a discrete number of particles is always used, the method is prone to encounter problems originating from subsampling. Smoothing techniques must be then used to improve the performance of the method and further reduce the number of particles [*Fernàndez-Garcia and Sanchez-Vila*, 2011]. Once the total density field $\rho_i(\mathbf{x}, t)$ is estimated, concentrations can be calculated as $c_i(\mathbf{x}, t) = \rho_i(\mathbf{x}, t)/(\phi(\mathbf{x})R_i(\mathbf{x}))$. The drift and dispersive terms in (36) were obtained neglecting boundary effects. Specific formulations should be derived to include the effect of boundaries on particles. Alternatively, one can switch the motion of a particle at the boundary so as to follow the standard random walk algorithm with a retardation factor determined by its initial state. This will require a more restrictive criterion in dt at that location (see section 6.3).

It is worth mentioning that the method can still be used when not all products in the reaction network are accounted for (e.g., the release of chlorides during reductive dechlorination) or when the reaction chain is truncated for simplification purposes (e.g., only PCE and TCE are considered in the simulation). In those cases, the total mass of the species considered will decrease with time and the columns in the state transition probability matrix will not sum to one, i.e., $\sum_{i=1}^{n_s} P_{ij} < 1$. This loss of mass in the chemical system due to the transformation of species into unspecified products can easily be considered in the algorithm by removing from the simulation those particles that satisfy that

$$r > \sum_{i=1}^{n_s} P_{ij}(t). \tag{38}$$

The method has advantages and limitations. The major limitation is that only contaminated sites with concentrations below the Michaelis half-saturation constant (in the pseudolinear regime) can be properly simulated. Monod or Michaelis-Menten enzyme kinetics should be used otherwise. The main advantage is that, under this condition, the transport problem is still linear and, consequently, the motion of a particle is independent from the type and density of particles nearby. This has several implications. Chief among them is that the particle tracking simulation can be executed one particle at a time (or in parallel) with a constant displacement (CD) scheme [*Wen and Gómez-Hernández*, 1996]. The CD scheme used here locally adapts the time step dt to satisfy a fixed courant number (Cu) at any given time and position,

$$\frac{\|\mathbf{q}\|}{\|\Delta\mathbf{s}\|}\frac{dt}{\phi R_{ij}^e} = Cu < 1, \tag{39}$$

where $\Delta\mathbf{s} = (dx, dy, dz)$ is the size of the grid cell. This maintains accuracy and efficiency in heterogeneous porous media. Otherwise, areas with small velocities can slow down the simulation [*Wen and Gómez-Hernández*, 1996].

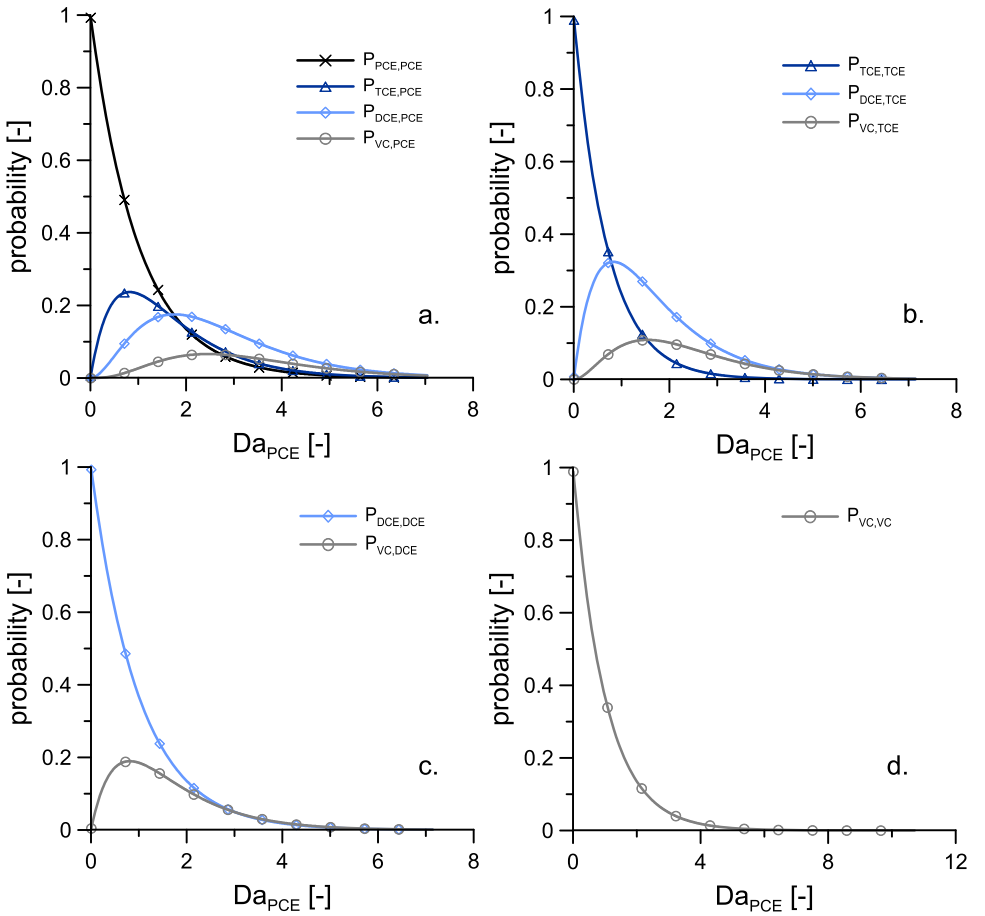

Figure 1. Transition probabilities as a function of the limiting Damköhler number for a particle initially belonging to species (a) PCE, (b) TCE, (c) DCE, and (d) VC. The parameters adopted to generate these probabilities are presented in Table 1.

6. Application to Parent-Daughter Serial Reactions

6.1. Analytical Solution

The particle tracking algorithm is here applied to simulate a serial reaction system. For instance, the sequential reductive dechlorination of the perchloroethylene (PCE → TCE → DCE → VC → 0). The nonzero components of the matrix **K** defining this chemical system can be written as

$$K_{ij} = -\frac{k_i}{R_i}, \quad \text{i=j} \quad \text{and} \quad K_{ij} = \frac{y_i k_j}{R_j}, \quad \text{j=i-1}, \quad \text{j} < \text{i} \tag{40}$$

Table 1. Chemical and Physical Parameters Used to Compare the New Particle Tracking Method With the Well-Known Finite Difference Transport Code RT3D

	Value			
Parameter	pce	tce	dce	vc
First-order decay, k_i (days)	0.05	0.03	0.02	0.015
Yield coefficient, $y_{i/j}$ (mol^{-1})	×	0.79	0.74	0.64
Retardation factor, R_i	7.1	2.9	2.8[a], 2.0[b]	1.4
Number of cells	500			
Cell dimension, (m)	1.0			
Longitudinal dispersivity (m)	0.5			
Darcy velocity (md^{-1})	0.3			
Porosity	0.3			

[a]Used for the comparison with RT3D in section 6.1 (Figures 1 and 2) and the 3-D simulations (Figures 11 and 12).
[b]Used to illustrate the normalized moments (Figures 3 and 4) and the effective parameters (Figures 5 and 6).

where y_i is the amount of species i produced from its immediate parent species $i-1$. Considering strictly a forward serial reaction, we are dealing here with a triangular matrix **K**, a mathematically convenient matrix form that allows us deriving an analytical expression of the eigensystem. Indeed, the eigenvalues of a triangular matrix are its diagonal elements, i.e., the diagonal matrix $\mathbf{K}'$ is expressed as $K'_{ii}=-k_i/R_i$. The columns vectors of the matrix **S** are the corresponding eigenvectors. The derivation shows a pattern that can be written for a generic number of species as

$$S_{ij}=S_{ij}^{-1}=0, \qquad j>i,$$

$$S_{ij}=S_{ij}^{-1}=1, \qquad j=i,$$

$$S_{ij}=R_i R_j^{i-j-1}\prod_{m=j}^{i-1}\left(\frac{k_m y_{m+1}}{R_j k_{m+1}-R_{m+1}k_j}\right),$$

$$S_{ij}^{-1}=R_i^{i-j}\prod_{m=j}^{i-1}\left(\frac{-k_m y_{m+1}}{R_m k_i-R_i k_m}\right).$$

Substituting these analytical expressions into (20)–(25) will provide transition probabilities and corresponding spatial moments with highest computational efficiency. Note that the analytical solution is theoretically applicable to any number of species involved in a serial reaction system.

Based on these results, Figure 1 displays the transition probabilities associated to a particle that initially belongs to species PCE (a), TCE (b), DCE (c) or VC (d). The parameters used resemble those typically obtained in the field and are summarized in Table 1. The time variable in the following figures is presented in

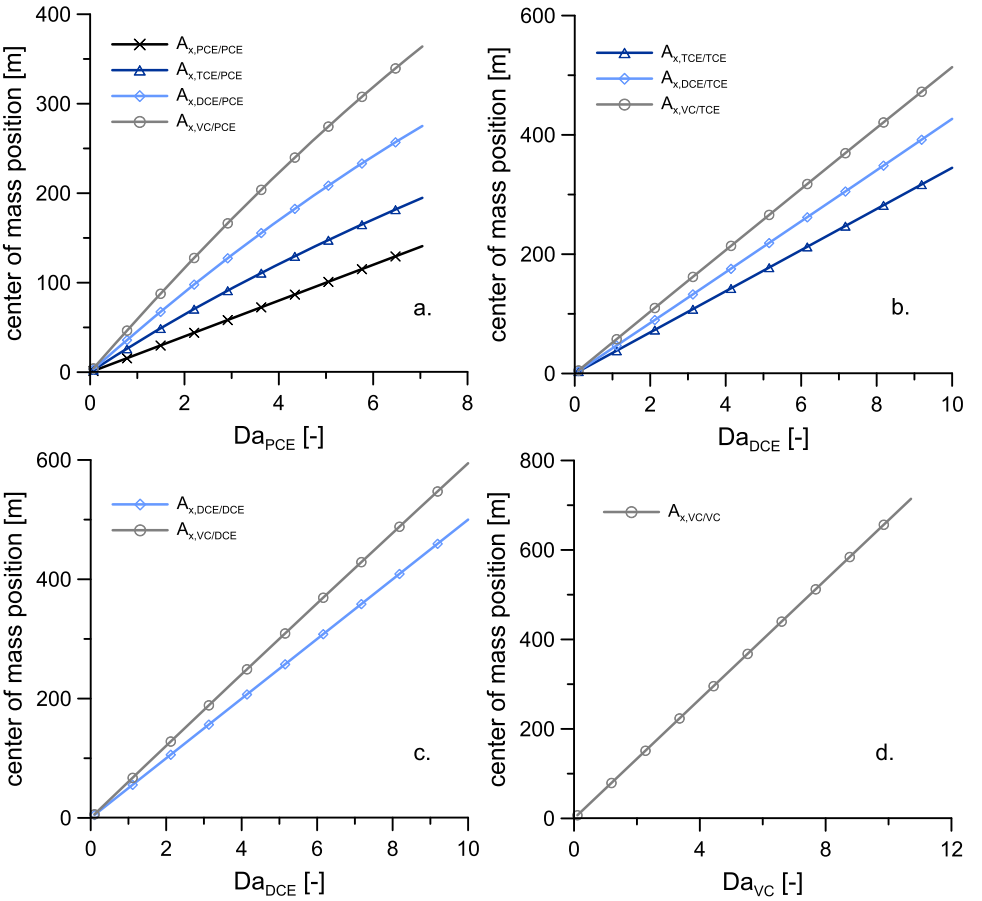

Figure 2. First normalized spatial moment as a function of the limiting Damköhler number for a particle initially belonging to species (a) PCE, (b) TCE, (c) DCE, and (d) VC.

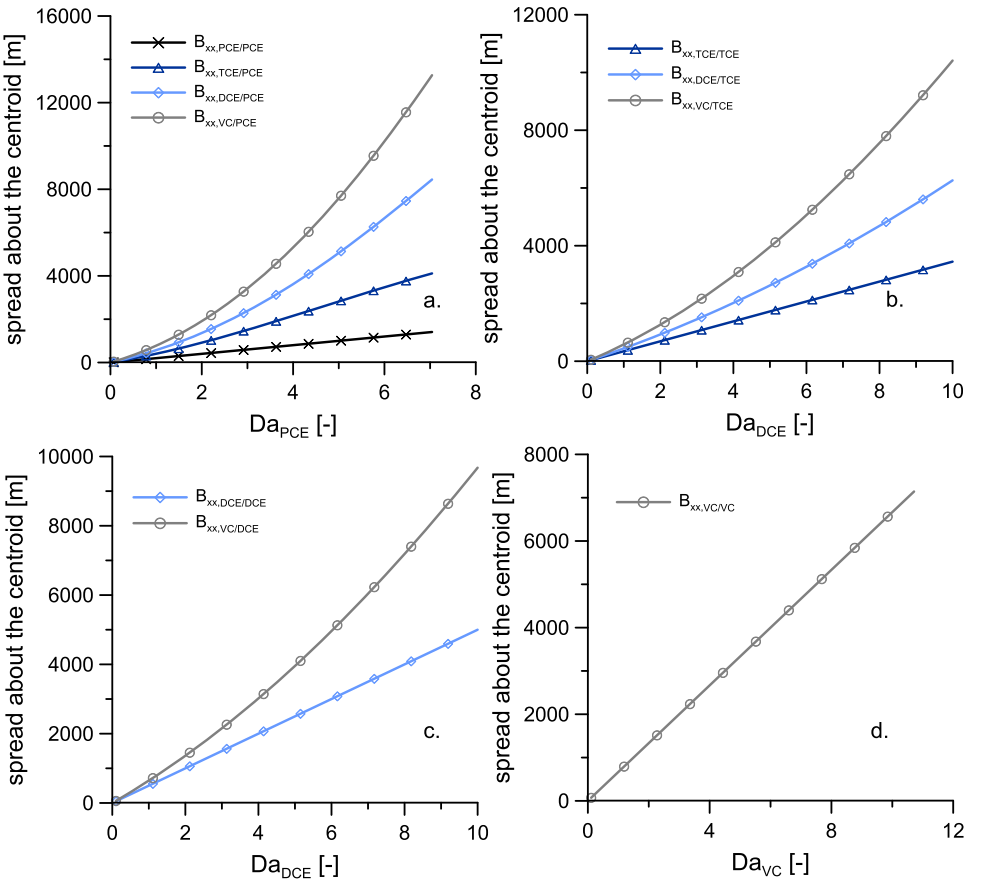

Figure 3. Second normalized spatial moment as a function of the limiting Damköhler number for a particle initially belonging to species (a) PCE, (b) TCE, (c) DCE, and (d) VC.

dimensionless form based on the limiting Damköhler number *Da* in the reaction chain. Given a particle initially belonging to species *j*, it is defined as

$$Da = \min\{k_j t/R_j, \ldots, k_{n_s} t/R_{n_s}\}. \tag{41}$$

Let us focus on Figure 1a. Interestingly, intermediate species such as TCE show two clear regimes. While at early times the probability of being TCE increases due to the biodegradation of its immediate parent species PCE, later on, this probability reaches a maximum and afterward vanishes due to its transformation into DCE. Similar behavior is also observed in other cases. Figures 3 and 4 show the corresponding center of mass and spread given by (24) and (25). Remarkably, since daughter species have smaller retardation factors ($R_{PCE} > R_{TCE} > R_{DCE} > R_{VC}$), particles that are transformed into daughter species reflect larger effective velocities. Thus, the effective velocity associated with the transformation of PCE into TCE is smaller than that of the transformation of PCE into DCE or VC.

The developed particle tracking algorithm was incorporated into the numerical random walk particle tracking code RW3D [*Fernàndez-Garcia et al.*, 2005a]. Figure 2 shows the simulation of the reductive dechlorination of PCE in a homogeneous one-dimensional system. The input parameters used are shown in Table 1. A total of 100,000 particles were used to simulate a punctual and instantaneous injection. Results are contrasted against those generated by the well-known finite difference code RT3D [*Clement*, 1997]. An excellent match is obtained.

6.2. Behavior of Effective Parameters

As previously shown in section 4, the expressions of the first and second spatial moments developed for a network reaction system (24) and (25) are similar to the classical random walk particle motion, provided that an effective retardation factor and an effective dispersion coefficient are properly introduced. Figure 5

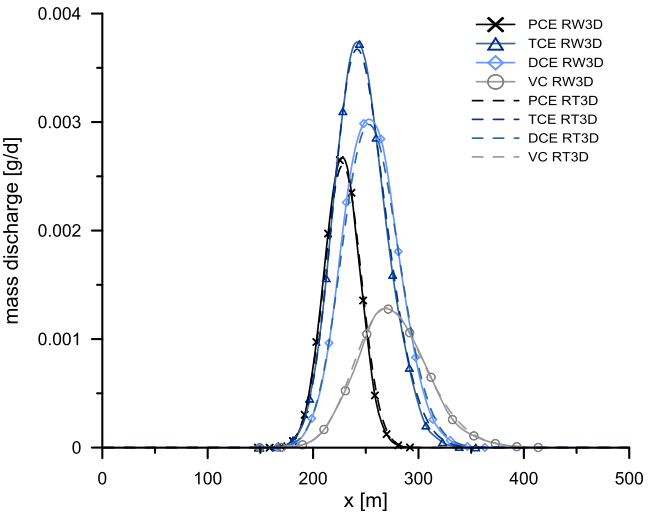

Figure 4. Comparison of the proposed particle tracking method with the RT3D code. Mass distribution as a function of distance obtained at $t = 200$ days resulting from a punctual and instantaneous injection of PCE in a homogeneous one-dimensional model.

shows the temporal behavior of the effective retardation factor R^e_{ij} for a serial reaction system (dechlorination of PCE). Suppose that a particle initially belonging to species *j* is transformed into species *i*. Results show that at small times the effective retardation factor is similar to the harmonic mean of the individual retardation factors of the species lying between *j* and *i*. This value is represented by $\hat{R}^e_{ij}$. On the other hand, at large times, the effective retardation tends to the retardation factor of the species having the highest expected life span, i.e., ratio of the retardation factor to the decay rate. This result can be physically interpreted by noticing that as time increases the less degradable species should persist and therefore govern the solution. Figure 5a shows the behavior of the effective retardation factor associated with a particle being initially PCE. Since PCE is the less degradable species in the reaction system (smallest k_{PCE}/R_{PCE} value), results demonstrate that the effective retardation factor comes close to R_{PCE} at large times for all species. On the other hand, for the same reason, when the initial species is TCE in Figure 5b (PCE does not exist), the effective retardation factor is similar to R_{DCE} at large times.

The temporal evolution of the effective dispersion coefficient is shown in Figure 6 for a serial reaction system. For the PCE-PCE transformation (no change in the particle species state), the spread of a particle reflects a normal diffusion-dispersive process, i.e., constant dispersion coefficient. However, for intermediate transformations such as PCE-TCE or PCE-DCE an interesting behavior is developed with different time regimes. Let us focus on PCE-DCE, as DCE is produced from the transformation of PCE into TCE and TCE into DCE, the effective dispersion coefficient rapidly increases with time approaching a maximum that exhibits a value larger than the dispersion coefficient. As time goes by, the natural attenuation of DCE destroys the effective dispersion coefficient and follows a rapid decay with time.

6.3. Performance Assessment

In this section the performance of four different implementations of our particle tracking solution are compared. These different strategies are then contrasted against a known reactive transport code, RT3D. The state transition probability matrix $\mathbf{P}(t)$ is always used to determine the change in chemical state but a different approximation of the first and second spatial moments is used in each numerical strategy. This will help studying the benefits of using higher-order spatial moments in terms of computational efficiency. The following algorithms were analyzed:

• **Model A**: The motion of particles follows the standard random walk algorithm with a retardation factor determined by its initial state,

$$\mathbf{A}_{ij}(dt) \approx \frac{\mathbf{q}_p dt}{\phi R_i}, \tag{42}$$

$$\mathbf{B}_{ij}(dt) \approx \frac{2\mathbf{D}\, dt}{R_i}. \tag{43}$$

• **Model B**: The motion of particles only incorporates an effective retardation factor in the drift term of the standard random walk algorithm,

$$\mathbf{A}_{ij}(dt) = \frac{\mathbf{q}_p dt}{\phi R^e_{ij}(dt)}, \tag{44}$$

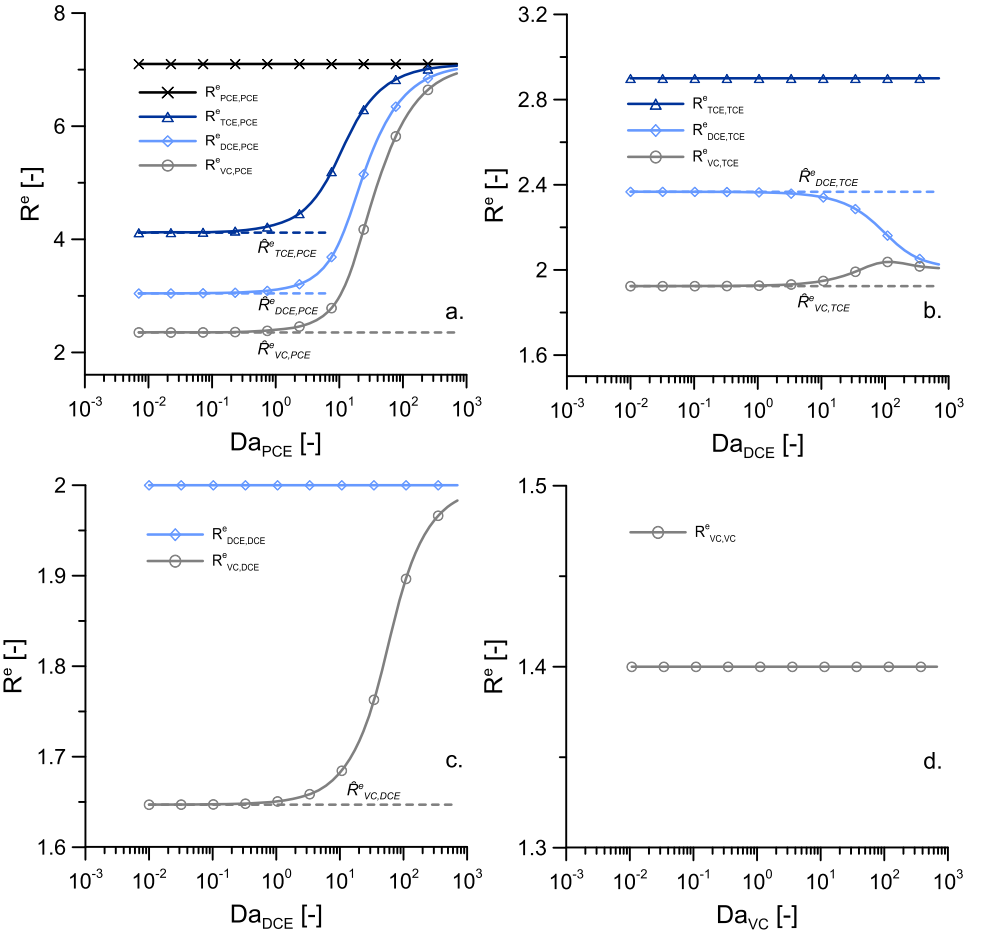

Figure 5. Effective retardation factor as a function of the limiting Damköhler number for a particle initially belonging to species (a) PCE, (b) TCE, (c) DCE, and (d) VC. The dashed lines represent the harmonic mean value.

$$\mathbf{B}_{ij}(dt) \approx \frac{2\mathbf{D}dt}{R_i}. \tag{45}$$

• **Model C**: The motion of particles incorporates both an effective retardation factor and an effective dispersion coefficient according to (24) and (25).

• **Model D**: The motion of particles follows the standard random walk algorithm with an effective retardation factor determined by the harmonic mean value $\hat{R}^e_{ij}$,

$$\mathbf{A}_{ij}(dt) \approx \frac{\mathbf{q}_p dt}{\phi \hat{R}^e_{ij}}, \tag{46}$$

$$\mathbf{B}_{ij}(dt) \approx \frac{2\mathbf{D}\,dt}{\hat{R}^e_{ij}}, \tag{47}$$

where

$$R^e_{ij}(dt) \approx \hat{R}^e_{ij} = (i-j+1)\left(\sum_{k=j}^{i} {R_k}^{-1}\right)^{-1}. \tag{48}$$

Consider a 200 meters long one-dimensional homogeneous problem with a groundwater velocity of 0.6 m/d and a longitudinal dispersivity of 0.5 m. The degradation of PCE into its daughter species (*PCE* → *TCE* → *DCE* → *VC*) is simulated. The parameters adopted are shown in Table 1. A substantial amount of PCE particles (200,000) was initially injected to reduce the effects of subsampling. The performance of the method is analyzed by estimating the normalized root mean square deviation (NRMSD) of the

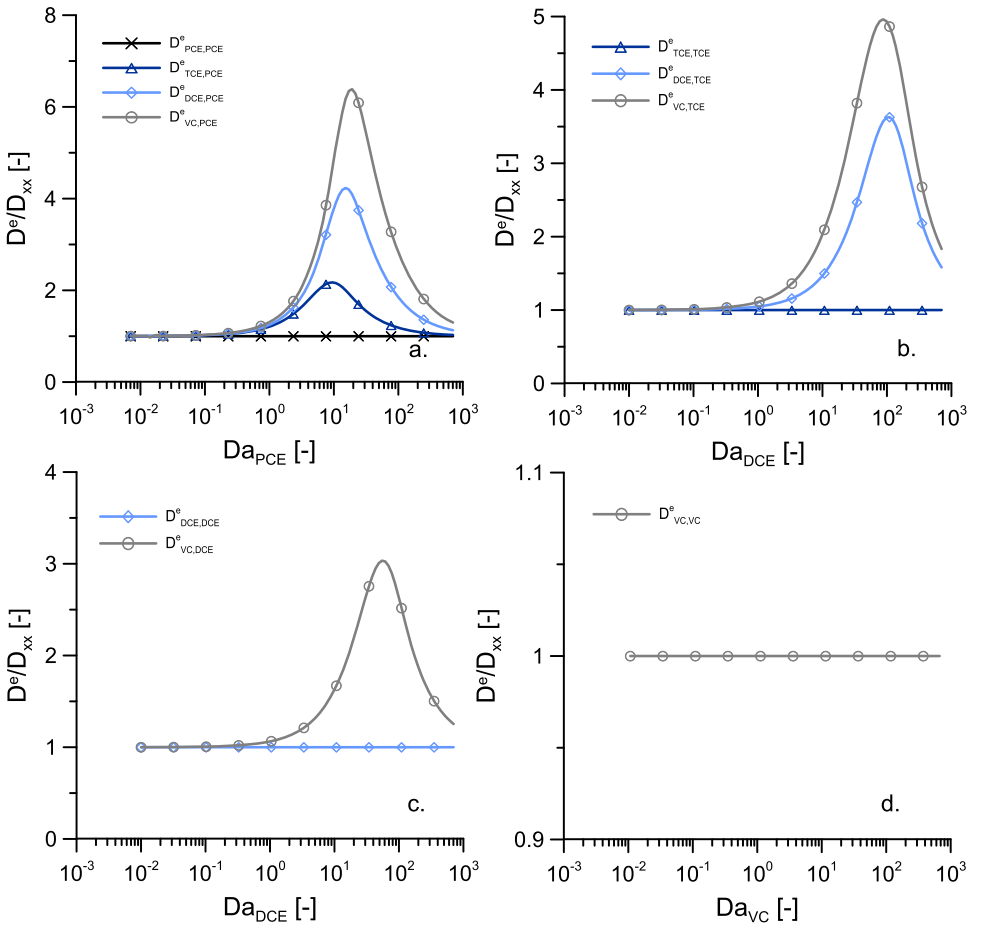

Figure 6. Normalized effective dispersion coefficient as a function of the limiting Damköhler number for a particle initially belonging to species (a) PCE, (b) TCE, (c) DCE, and (d) VC.

number of particles of TCE observed after 200 days in different block areas of the domain. The NRMSD is estimated by

$$NRMSD(dt) = \sqrt{\frac{1}{nb}\sum_{i=1}^{nb}\left(\frac{np_{sim,i}(dt) - np_{ref,i}}{np_{ref,i}}\right)^2}, \tag{49}$$

where $np_{sim,i}$ is the number of TCE particles observed in the ith block, np_{ref} is the reference number of TCE particles obtained using the random walk method with a very small time step, and nb is the total number of blocks used to discretized the domain ($nb = 200$). Figure 7 shows the normalized root mean square deviation as a function of the time step dt used in the random walk. The time step is written in terms of the Damköhler number, i.e., $Da = k_{PCE}dt/R_{PCE}$.

As expected, we note a clear improvement of the solution with decreasing time step and usage of higher spatial moments. For a given time step, Model C is more accurate than Models A and B. Interestingly, the differences between Model A and Model B (addition of first moments) are substantially larger than those observed between Model B and C (addition of second central moments). This suggests that the spatial moments of order higher than two are somehow redundant in practice. Moreover, the application of the harmonic mean in Model D reflects very accurate results with less computational effort compare to Model B and C.

Results also show that when the time step leads to a limiting Damköhler number Da smaller than 0.05 the use of only transition probabilities in Model A is sufficient to obtain accurate results. From a computational perspective, if higher spatial moments are considered (Model B and C), the time step in the random walk method can be larger than usual, drastically increasing its computational efficiency. Thus, in comparison to Model A,

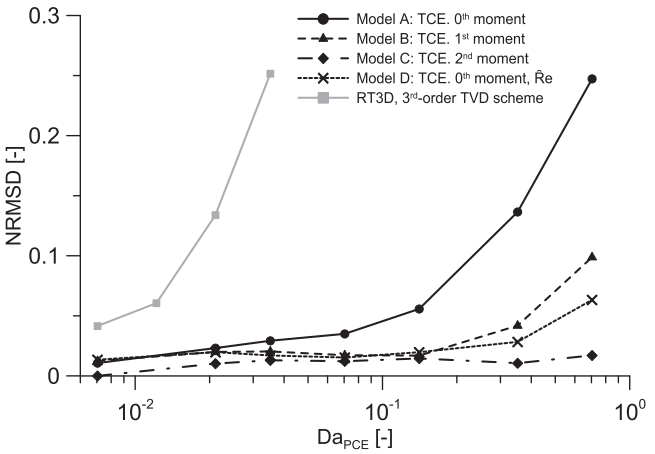

Figure 7. Normalized root mean square deviation (NRMSD) as a function of the time step used in the random walk simulation for the different model implementations: (a) Model A–zeroth moment; (b) Model B - 0th and 1st moments; (c) Model C–zeroth, first, and second moments; and (d) Model D–approximation of the effective retardation coefficient by the harmonic mean. The gray line gives the NRMSD for the finite difference code RT3D with the third-order TVD scheme to solve advection.

Model B and C can use larger *Da* values without additional computational effort. Interestingly, a simple approximation of the effective retardation factor by the harmonic mean (Model D) provides more accurate results than Model B. In this case, the limiting Damköhler number should be smaller than about 0.5.

The performance of our particle tracking method was then compared to a highly discretized finite-difference model. To do this, we chose to use the RT3D code, which has been widely employed in field applications for modeling bioremediation reactions. However, we note that RT3D simulates chemical reactions through an Operator-Split numerical strategy. Therefore, results shown here cannot be directly extrapolated to other numerical strategies. The setup of the simulations is the same as before with a Péclet number of 240 (advective-dominated). Among the several advection solvers available in RT3D, the ULTIMATE-TVD scheme was employed, which preserves monotonicity and avoids spurious oscillations in sharp fronts. The grey line shown in Figure 7 displays the NRMSD generated by the RT3D-TVD scheme. Here solute concentrations obtained from RT3D were converted into particles to be able to apply (49) in a similar fashion. Results demonstrate that, in this flow regime, the authors' particle approach produces always more accurate results than the RT3D-TVD scheme. This effect drastically increases with the time step employed. A close look at the results is provided in Figure 8, which shows the corresponding concentration profiles of PCE and TCE for different time step sizes. Remarkably, in this figure, one can clearly see that even though the RT3D-TVD scheme is capable of properly predicting conservative species (Figure 8a), the corresponding PCE and TCE concentrations (Figures 8b and 8c) exhibit numerical dispersion artifacts that increase with the time step size. This illustrates the high sensitivity of the operator-splitting finite difference method to generate numerical artifacts in reactive transport modeling. Effect that seems not to vanish even for small *Da* close to 0.01. On the contrary, our particle tracking approach is demonstrated to be numerically robust over a wide range of conditions.

7. Reductive Dechlorination of PCE in a 3-D Highly Heterogeneous System: An Example

The proposed method can efficiently model complex network reactions without restrictions in the spatial variability of the parameters. To illustrate this, a three-dimensional synthetic example of the effect of heterogeneity on the dechlorination of organic solvents is provided at a high resolution. Thus, the biotransformation of PCE into its daughter products TCE, DCE and VC are considered.

For this purpose, one realization of a sequential Gaussian simulation was chosen to describe the spatial variability of the hydraulic conductivity in an aquifer. The natural log of the hydraulic conductivity is represented by a zero mean random function associated with an isotropic spherical variogram characterized with a range a of 17 m and a variance of 2. For simplicity, all other parameters were assumed to be constant. The domain extends over an area of $L_x = 300$ m, $L_y = 180$ m, and $L_z = 120$ m, which is discretized into cells of size $\Delta x = \Delta y = \Delta z = 1.0$ m. This represents a 6.48 Million cells simulation. Figure 9 shows a sketch of the simulation setup. A confined aquifer driven by a mean uniform hydraulic gradient of 0.3 oriented along the x direction is considered. The flow problem is solved by means of the well known finite difference code, MODFLOW [*Harbaugh et al*., 2000]. This velocity field is then introduced into the particle tracking code, RW3D. A CD scheme [*Wen and Gómez-Hernández*, 1996] with $Cu = 0.1$ is employed to decrease

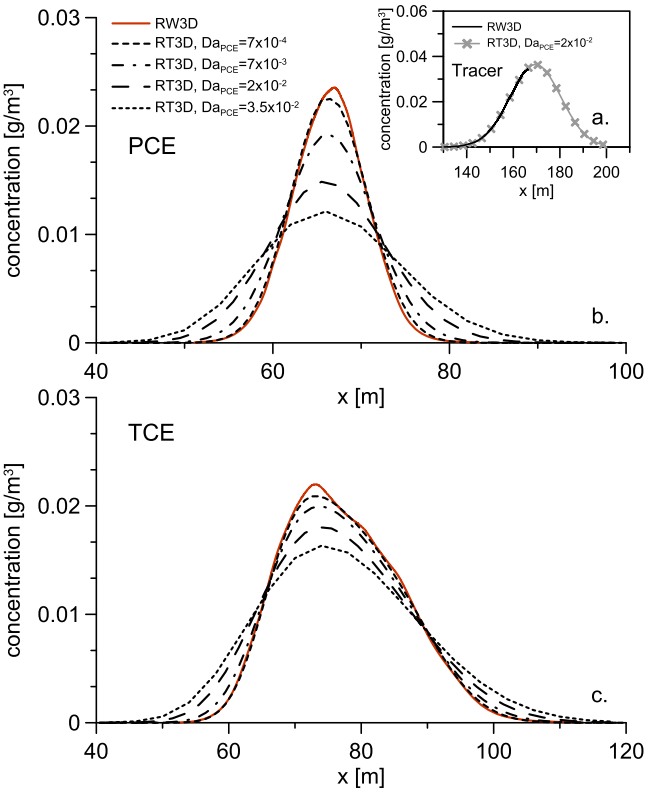

Figure 8. (a) Tracer, (b) PCE, and (c) TCE concentrations profile using the random walk method and the finite difference solution RT3D with different Damköhler number.

computational effort. All simulations were executed by the combination MODFLOW/RW3D, which takes advantage of the proposed algorithm.

Solute transport was simulated by releasing 100, 000 PCE particles randomly distributed in a vertical plane rectangular area of 34 m width and 17 m height located at $x = 80$ m (an injection that extends 2×1 ranges). The total mass injected was one unit. Three control planes situated at 2, 5 and 10 ranges from the injection location (corresponding to $x = 114$ m, 165 m and 250 m) were used to measure the mass flux breakthrough curves (BTCs) of all species. Subsampling effects were mitigated by reconstructing each BTC from the particle travel time distribution using an adaptive kernel density estimator method [*Pedretti and Fernàndez-Garcia*, 2013b]. Input chemical and physical parameters are summarized in Tables 1 and 2. A purely conservative tracer was also simulated with the same number of particles for comparison purposes.

7.1. Computational Efficiency

The computational efficiency of our particle tracking method is demonstrated through an estimation of CPU times and numerical accuracy. Figure 10 shows the CPU time required in the particle tracking simulation as a function of the number of particles injected for the four different model implementations used.

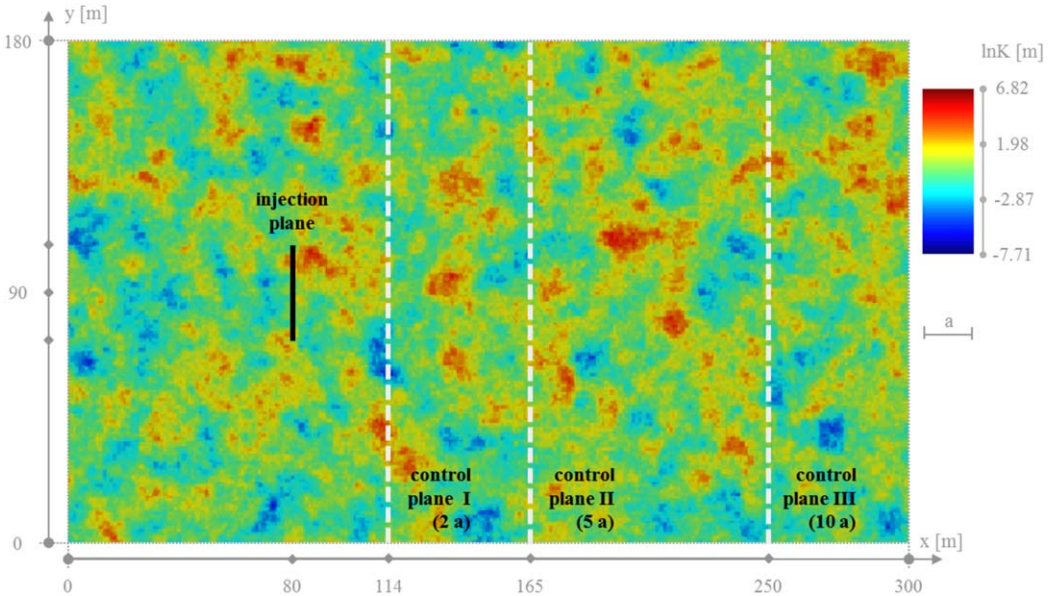

Figure 9. Aerial view of the randomly distributed hydraulic conductivity field with the location of the injection and control planes.

Table 2. Physical Parameters Adopted for Simulating Serial Reaction Transport in a 3-D Heterogeneous Porous Medium

Parameter	Value
Flow Problem	
Average hydraulic gradient	0.3
Longitudinal dispersivity, α_L (m)	0.04
Transversal dispersivity in the horizontal plane, α_{TH} (m)	0.004
Transversal dispersivity in the vertical plane, α_{TV} (m)	0.001
Porosity, ϕ	0.3
Heterogeneous Field	
Variogram type	spherical
Geometric mean of K (m^2/d)	1.0
Variance of ln K	2.0
Range, a (m)	17.0
Domain Discretization	
Number of cells in x direction, n_x	300
Number of cells in y direction, n_y	180
Number of cells in z direction, n_z	120
Cell dimension, $\Delta_x \times \Delta_y \times \Delta_z$ (m×m×m)	1.0 × 1.0 × 1.0

CPU times were obtained with a typical desktop computer (Intel(R) Xeon(R) CPU with 2.67 GHz and 3GB of RAM memory). These results are contrasted against the mean relative mass discharge error (RME) of the species breakthrough curves determined by,

$$RME(x) = \left(\frac{1}{n_s n_t} \sum_{j=1}^{n_t} \sum_{i=1}^{n_s} E_i^2(t_j; x) \right)^{1/2}, \quad (50)$$

where

$$E_i(t; x) = \frac{Q_{sim,i}(t; x) - Q_{ref,i}(t; x)}{Q_{ref,i}(t; x)}. \quad (51)$$

Here $Q_{sim,i}(t; x)$ is the cumulative breakthrough curve of the ith species obtained at the $x = 250$ control plane, $Q_{ref,i}(t; x)$ is the corresponding reference cumulative breakthrough curve obtained by injecting a large number of particles (10^5) in model C, $E_i(t; x)$ is the relative error associated with the cumulative breakthrough curve of the ith species obtained at $x = 250$ and time t, and n_t is the number of discrete times in the cumulative breakthrough curve. Figure 10 shows that the proposed method is capable to solve a finely discretized heterogeneous multicomponent reactive transport model in a relatively small range of CPU times (less than 15 min for 10^5 particles). CPU time increases linearly with the number of particles. The choice of the number of particles will determine the accuracy of the solution. Results also illustrate the gain in computational efficiency given by an approximate solution of the effective retardation and dispersion parameters (Model A and D). The small benefit in numerical accuracy granted by the use of higher moments in this case is consistent with our previously analysis (see Figure 7). In this case, the CD scheme, which adapts the time step to local velocities based on the grid courant number Cu, led to sufficiently small Damköhler numbers ($Da < 0.01$).

7.2. Importance of Heterogeneity

The effect of heterogeneity is demonstrated by comparing the heterogeneous solution with an equivalent homogeneous one obtained with apparent transport parameters. These apparent parameters were estimated from the first two temporal moments of the heterogeneous tracer breakthrough curves (parameters given in Table 3). The resulting BTCs are shown in Figure 11. The figures on the left display the heterogeneous solutions obtained at three control planes while the figures on the right illustrate the corresponding homogeneous solutions. The simulated tracer BTCs in the heterogenous system are highly asymmetric (positively skewed) and characterized by a marked peak and a power-law behavior at late times similar to $c \sim t^{-1.4}$. This effect is clearly developed in the second control plane (5 ranges from the injection location) and seems to vanish from then on. Field and laboratory evidence of power-law behavior resulting from the effect of heterogeneity is significant [*Hoehn et al.*, 1998; *Haggerty et al.*, 2000; *Fernàndez-Garcia et al.*, 2004; *Gouze et al.*, 2008]. In the field, the power-law exponent typically falls anywhere between one and three [*Haggerty et al.*, 2000]. The results of this study are consistent

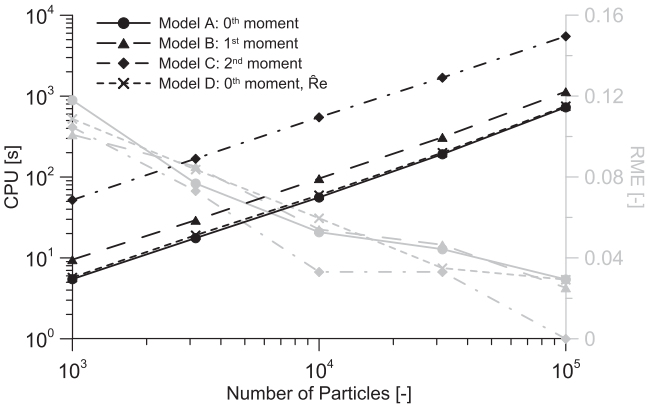

Figure 10. CPU time and mean relative mass discharge error (RME) as a function of the number of particles used in the random walk simulations for the four different model implementations.

Table 3. Apparent Parameters Used to Simulate Equivalent Homogeneous Solutions at the Three Different Control Planes

	Value at		
Parameter	plane 2a	plane 5a	plane 10a
Velocity, v (m/d)	0.736	0.942	0.935
Longitudinal dispersivity, α_L (m)	9.457	8.245	8.355
Transversal dispersivity in the horizontal plane, α_{TH} (m)	0.181	0.158	0.247
Transversal dispersivity in the vertical plane, α_{TV} (m)	0.098	0.207	0.133

with field observations and demonstrate that power law distributions appear naturally in heterogeneous porous media, provided that a full three-dimensional model is used. Similar results on the formation of BTCs tailing during convergent flow tracer tests have been recently reported by *Pedretti et al*. [2013a].

The BTCs of the reactive species show an interesting different behavior of the late-time distribution. In fact, biodegradation seems to hinder the formation of power law tailing. BTCs are still highly asymmetric but there is not a clear regime in which a power law distribution is manifested. This can be attributed to the following processes: (1) Since particles can partially react and produce new species, the slow particles that otherwise may develop tailing can now be transformed into other species; (2) the production and destruction of the different species is not instantaneous but evolve with time in a complex manner, and (3) First-order kinetics results in exponentially decaying concentrations that obscures the sole effect of heterogeneity leading to late-time power law behavior.

At short distances (few travel ranges), important nonnegligible differences can be observed between the homogeneous and heterogeneous solution. Results show that the equivalent homogeneous model leads to erroneous predictions of the reactive species BTCs, which led to earlier arrival times and substantial

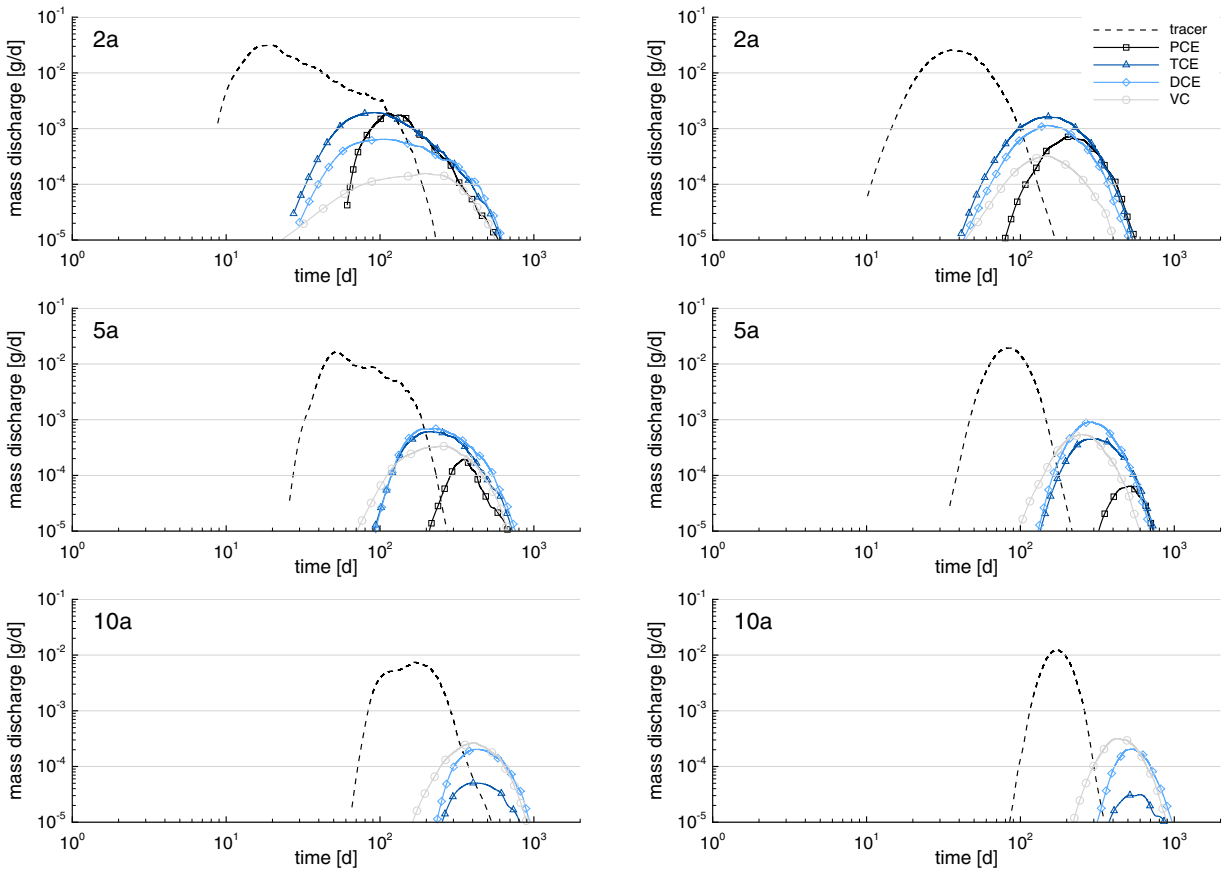

Figure 11. Breakthrough curves of PCE, TCE, DCE, and VC obtained at 2, 5, and 10 ranges (distance from injection) in (left) a 3-D heterogeneous porous medium and (right) an equivalent homogeneous porous medium.

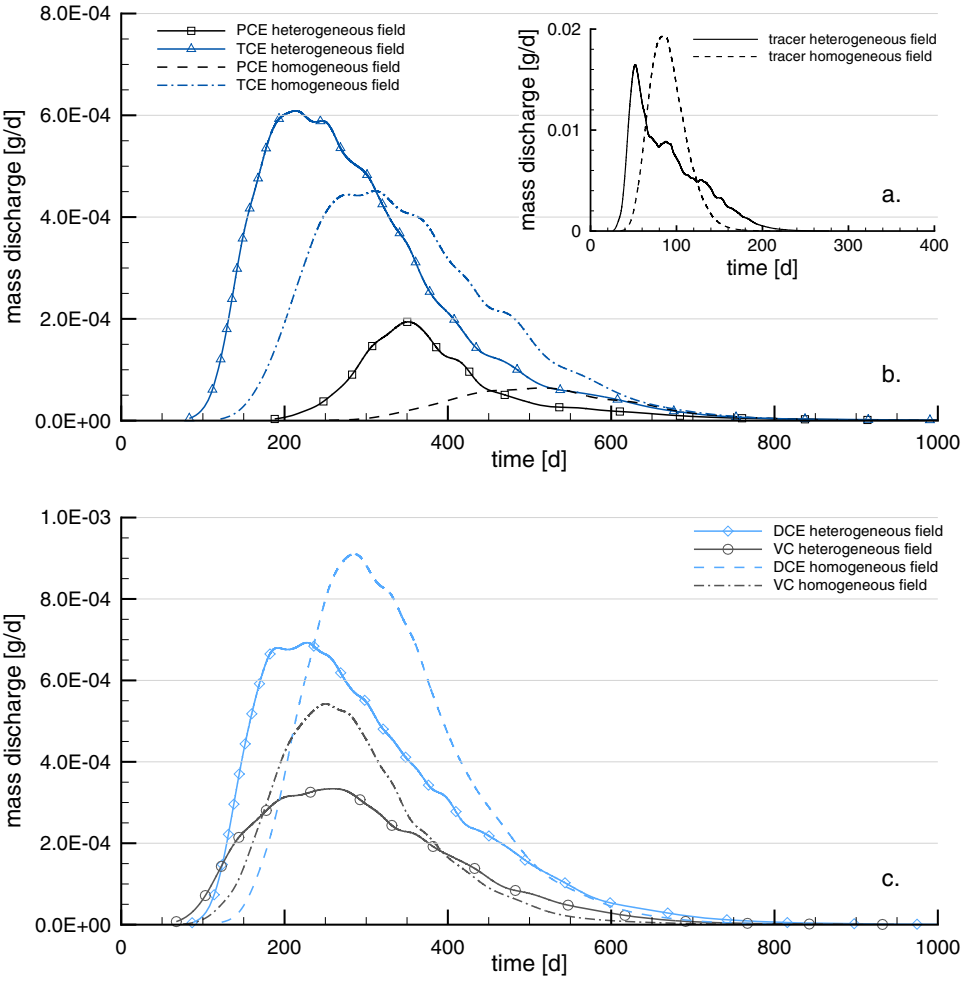

Figure 12. Comparison of the breakthrough curves simulated with the heterogeneous and homogeneous model at a distance of 5 ranges from the injection.

differences in the peak of concentrations, i.e., smaller PCE and TCE peak concentrations but significantly larger DCE and VC peak concentrations. This is further illustrated in Figure 12, which shows the BTCs obtained at $x=5a$ in a linear scale. Taking into account that VC is highly toxic compared to the other daughter species, the approximated consideration of the aquifer as effectively homogeneous can sorely mistake the estimation of risk, an assumption that is typically preferred by decision makers.

8. Conclusion

The authors have developed a new particle tracking method to efficiently simulate, without restrictions in the spatial variability of biochemical and physical parameters, the behavior of a multispecies contaminant plume affected by reaction networks. The approach is limited to pseudofirst-order kinetics. This is important for assessing the risk posed by a large variety of chlorinated organic compounds that otherwise suffer from numerical problems in dealing with heterogeneities. The new algorithm can be easily integrated into any standard random walk code and is obtained from the solution matrix of the spatial moments governing equations.

Results have illustrated the interplay between biochemical reactions and the advective-dispersive particle motion. In particular, the motion of a particle has been shown to follow a standard random walk with effective parameters. These effective parameters depend on the initial and final chemical state of a particle and evolve with time as a result of differential retardation effects among species.

Explicit analytic solutions of the transition probability matrix and related particle motions have been provided for serial reactions. In this case, the behavior of the effective retardation factor at short travel

distances has been determined to be efficiently approximated by the harmonic mean of the species lying between the initial and final chemical state. This approximation can substantially speed up the transport simulation that should guarantee that the limiting Damköhler number is smaller than 0.5 to maintain accuracy. At large times, the effective retardation factor has been shown to approach the retardation factor of the less degradable species. The effective dispersion coefficient has a production and a destruction term determined by the degradation of parent and daughter species, respectively.

A three-dimensional example of the effect of heterogeneity on the dechlorination of organic solvents is provided at a high resolution to illustrate the capabilities of the method. The example has demonstrated that the method presented constitutes a valuable tool for the evaluation of linear network reactions in complex systems, being capable of solving a finely discretized heterogeneous multicomponent reactive transport model efficiently with a regular desktop computer using relatively small CPU times. Interestingly, simulations have also shown that the power-law behavior typically observed in non-reactive tracer breakthrough curves can be largely compromised by the effect of biochemical reactions. In contrast to the clear power law behavior observed for nonreactive tracers in the same field, the corresponding breakthrough curves associated with reactive species exhibited highly asymmetric shapes without a clear regime in which a power law distribution is manifested.

Appendix A : Derivation of First Spatial Moments

From equation (16), the solution matrix of the absolute first spatial moment (x direction) satisfies the following system of ordinary differential equations

$$\frac{d\mathbf{X}_x}{dt} = \frac{q'_x}{\phi}\mathbf{R}^{-1}\mathbf{P}(t)+\mathbf{K}\mathbf{X}_x, \tag{A1}$$

subject to the initial condition

$$\mathbf{X}_x(t=0)=\mathbf{0} \tag{A2}$$

where the matrix $\mathbf{X}_x$ is the $n_s \times n_s$ absolute first spatial moment matrix. The matrix $\mathbf{R}^{-1}$ is a diagonal matrix composed by the inverse of the retardation factors, and $\mathbf{K}$ is the reaction matrix. The parameter q'_x and ϕ represent the particle Darcy velocity in the x direction and the porosity of the medium, respectively. $\mathbf{P}(t)$ is the species state transition probability matrix. Defining the matrix $\mathbf{Y}_x(t)$ by

$$\mathbf{Y}_x(t)= \frac{q'_x}{\phi}\mathbf{R}^{-1}\mathbf{P}(t), \tag{A3}$$

leads to the following system of equations

$$\frac{d\mathbf{X}_x}{dt} =\mathbf{Y}_x(t)+\mathbf{K}\mathbf{X}_x, \tag{A4}$$

whose solution is

$$\mathbf{X}_x(t)=\int_0^t \exp\left(\mathbf{K}(t-s)\right)\mathbf{Y}_x(s)ds. \tag{A5}$$

After the diagonalization of $\mathbf{K}$ by $\mathbf{K}=\mathbf{S}\mathbf{K}'\mathbf{S}^{-1}$, the solution can be written as

$$\mathbf{X}_x(t)=\int_0^t \mathbf{S}\exp\left(\mathbf{K}'(t-s)\right)\mathbf{S}^{-1}\mathbf{Y}_x(s)ds, \tag{A6}$$

where $\mathbf{S}$ is the transformation matrix composed by the eigenvalues of the reaction matrix $\mathbf{K}$, and $\mathbf{K}'$ is the diagonal matrix whose components are the eigenvalues of $\mathbf{K}$. The component $X_{x,ij}$ of this matrix (A6) is expressed as

$$X_{x,ij}(t)=\sum_{p,q=1}^{n_s} S_{ip}S_{pq}^{-1}\int_0^t \exp\left(K'_{pp}(t-s)\right)Y_{x,qj}(s)ds, \tag{A7}$$

where

$$Y_{x,qj}(s)=\frac{q'_x}{\phi R_{qq}}P_{qj}(s). \tag{A8}$$

From (20), the species state transition probability matrix can also be expressed in terms of the eigenvalues and eigenvectors of **K** by

$$P_{qj}(s)=\sum_r S_{qr}\exp(K'_{rr}s)S^{-1}_{rj}. \tag{A9}$$

The first absolute moment of a particle plume that moves from species *j* to species *i* after a time interval *t* can be obtained by respectively introducing (A9) and (A8) into (A8) and (A7),

$$X_{x,ij}(t)=\frac{q'_x t}{\phi}\sum_{p,q,r=1}^{n_s}\frac{S_{ip}S^{-1}_{pq}S_{qr}S^{-1}_{rj}}{R_{qq}}F_{pr}(t), \tag{A10}$$

where

$$F_{pr}(t)=\frac{1}{t}\int_0^t \exp(K'_{pp}(t-s))\exp(K'_{rr}s)ds. \tag{A11}$$

The solution of this integral is

$$F_{pr}(t)=\begin{cases}\dfrac{\exp(K'_{pp}t)-\exp(K'_{rr}t)}{t(K'_{pp}-K'_{rr})}, & \text{if } p\neq r\\ \exp(K'_{rr}t), & \text{if } p=r\end{cases} \tag{A12}$$

Based on this, the normalized first absolute spatial moments can be written as

$$A_{ij,x}(t)=\frac{X_{x,ij}}{P_{ij}}=\frac{q'_x t}{\phi R^e_{ij}(t)}, \tag{A13}$$

where $R^e_{ij}(t)$ is an effective retardation coefficient defined by

$$\frac{1}{R^e_{ij}(t)}=\frac{1}{P_{ij}(t)}\sum_{p,q,r=1}^{n_s}\frac{S_{ip}S^{-1}_{pq}S_{qr}S^{-1}_{rj}}{R_{qq}}F_{pr}(t). \tag{A14}$$

Appendix B : Derivation of Second Spatial Moments

From equation (17), the solution matrix of the absolute second spatial moment (*xy* component) satisfies the following system of ordinary differential equations

$$\frac{d\boldsymbol{\Psi}_{xy}}{dt}=\frac{q'_y}{\phi}\mathbf{R}^{-1}\mathbf{X}_x+\frac{q'_x}{\phi}\mathbf{R}^{-1}\mathbf{X}_y+2D_{xy}\mathbf{R}^{-1}\mathbf{P}+\mathbf{K}\boldsymbol{\Psi}_{xy}, \tag{B1}$$

subject to the initial condition

$$\boldsymbol{\Psi}_{xy}(t=0)=\mathbf{0} \tag{B2}$$

where the component $\Psi_{xy,ij}$ represents the temporal evolution of the absolute second moment of a particle plume originally belonging to species *j* and turning into species *i* in the time interval *t*. Defining

$$\mathbf{Y}_{xy}(t)=\frac{q'_y}{\phi}\mathbf{R}^{-1}\mathbf{X}_x+\frac{q'_x}{\phi}\mathbf{R}^{-1}\mathbf{X}_y+2D_{xy}\mathbf{R}^{-1}\mathbf{P}, \tag{B3}$$

we obtain the following inhomogeneous first-order linear differential equation system

$$\frac{\partial\boldsymbol{\Psi}_{xy}}{\partial t}=\mathbf{Y}_{xy}(t)+\mathbf{K}\boldsymbol{\Psi}_{xy}(t). \tag{B4}$$

The solution of (B4) is

$$\mathbf{\Psi}_{xy}(t)=\int_0^t \exp\left(\mathbf{K}(t-s)\right)\mathbf{Y}_{xy}(s)ds. \tag{B5}$$

After the diagonalization of $\mathbf{K}$ by $\mathbf{K}=\mathbf{S}\mathbf{K}'\mathbf{S}^{-1}$, this solution can be written as

$$\mathbf{\Psi}_{xy}(t)=\int_0^t \mathbf{S}\exp\left(\mathbf{K}'(t-s)\right)\mathbf{S}^{-1}\mathbf{Y}_{xy}(s)ds, \tag{B6}$$

where $\mathbf{S}$ is the transformation matrix composed by the eigenvalues of the reaction matrix $\mathbf{K}$, and $\mathbf{K}'$ is the diagonal matrix whose components are the eigenvalues of $\mathbf{K}$. The component $\Psi_{xy,ij}$ of this matrix (B6) can be expressed as

$$\Psi_{xy,ij}(t)=\sum_{a,b=1}^{n_s} S_{ia}S_{ab}^{-1}\int_0^t \exp\left(K'_{aa}(t-s)\right)Y_{xy,bj}(s)ds. \tag{B7}$$

From (B3), the component $Y_{xy,bj}$ is

$$Y_{xy,bj}(s)=\frac{q'_y}{\phi R_{bb}}X_{x,bj}(s)+\frac{q'_x}{\phi R_{bb}}X_{y,bj}(s)+\frac{2D_{xy}}{R_{bb}}P_{bj}(s). \tag{B8}$$

Substituting (A9) and (A10) into (B8) and (B7) we obtain

$$\Psi_{xy,ij}(t)=2D_{xy}t\sum_{a,b,u=1}^{n_s}\frac{S_{ia}S_{ab}^{-1}S_{bu}S_{uj}^{-1}}{R_{bb}}F_{au}(t)+\frac{2q'_xq'_yt^2}{\phi^2}\sum_{a,b,p,q,r=1}^{n_s}\frac{S_{ia}S_{ab}^{-1}S_{bp}S_{pq}^{-1}S_{qr}S_{rj}^{-1}}{R_{bb}R_{qq}}H_{apr}(t), \tag{B9}$$

where $F_{au}(t)$ is defined in (A12) and $H_{apr}(t)$ is

$$H_{apr}(t)=\frac{1}{t^2}\int_0^t \exp\left(K'_{aa}(t-s)\right)sF_{pr}(s)ds. \tag{B10}$$

The solution of this integral can be written as

$$H_{apr}(t)=\begin{cases}\dfrac{F_{ap}(t)-F_{ar}(t)}{t\left(K'_{pp}-K'_{rr}\right)}, & \text{if } p\neq r\\ W_{ar}(t), & \text{if } p=r\end{cases} \tag{B11}$$

where

$$W_{ar}(t)=\begin{cases}\dfrac{\exp\left(K'_{rr}t\right)\left[\left(K'_{rr}-K'_{aa}\right)t-1\right]+\exp\left(K'_{aa}t\right)}{t^2\left(K'_{aa}-K'_{rr}\right)^2}, & \text{if } a\neq r\\ \exp\left(K'_{aa}t\right)/2, & \text{if } a=r\end{cases} \tag{B12}$$

Based on this, the normalized second absolute spatial moment can be written as

$$B'_{xy,ij}(t)=\frac{2D_{xy}}{R^e_{ij}(t)}t+\frac{2q'_xq'_y}{\phi^2G_{ij}(t)}t^2, \tag{B13}$$

where

$$G_{ij}(t)=P_{ij}(t)\left(\sum_{a,b,p,q,r=1}^{n_s}\frac{S_{ia}S_{ab}^{-1}S_{bp}S_{pq}^{-1}S_{qr}S_{rj}^{-1}}{R_{bb}R_{qq}}H_{apr}(t)\right)^{-1}. \tag{B14}$$

Knowing (22) and (A13), the second central spatial moment is

$$B_{xy,ij}(t)=\frac{2D_{xy}}{R^e_{ij}(t)}t+\frac{2q'_xq'_y}{\phi^2R^e_{ij}(t)}\left(\frac{R^e_{ij}(t)}{G_{ij}(t)}-\frac{1}{2R^e_{ij}(t)}\right)t^2. \tag{B15}$$

Acknowledgments
The authors acknowledge the financial support provided by the Spanish Ministry of Science and Innovation through the SCARCE Consolider-Ingenio 2010 program (reference CSD2009-00065) and the project FEAR (CGL2012-38120).

References

Allen-King, R. M., D. P. Divine, M. J. L. Robin, J. R. Alldredge, and D. R. Gaylord (2006), Spatial distributions of perchloroethylene reactive transport parameters in the Borden Aquifer, *Water Resour. Res.*, *42*, W01413, doi:10.1029/2005WR003977.

Andričević, R., and E. Foufoula-Georgiou (1991), Modeling kinetic non-equilibrium using the first two moments of residence time distribution, *Stochastic Hydrol. Hydraul.*, *5*, 155–171.

Bagtzoglou, A., A. F. B. Tompson, and D. E. Dougherty (1992), Projection functions for particle grid methods, *Numer. Methods Partial Differential Equations*, *8*, 325–340.

Benekos, I. D., C. A. Shoemaker, and J. R. Stedinger (2006), Probabilistic risk and uncertainty analysis for bioremediation of four chlorinated ethenes in groundwater, *Stochastic Environ. Res. Risk Assess.*, *21*(4), 375–390, doi:10.1007/s00477-006-0071-4.
Benson, D. A., and M. M. Meerschaert (2008), Simulation of chemical reaction via particle tracking: Diffusion-limited versus thermodynamic rate-limited regimes, *Water Resour. Res.*, *44*, W12201, doi:10.1029/2008WR007111.
Benson, D. A., and M. M. Meerschaert (2009), A simple and efficient random walk solution of multi-rate mobile/immobile mass transport equations, *Adv. Water Res.*, *32*, 532–539.
Berkowitz, B., A. Cortis, M. Dentz, and H. Scher (2006), Modeling non-Fickian transport in geological formations as a continuous time random walk, *Rev. Geophys.*, *44*, RG2003, doi:10.1029/2005RG000178.
Bolster, D., M. Barahona, M. Dentz, D. Fernàndez-Garcia, X. Sanchez-Vila, P. Trinchero, C. Valhondo, and D. M. Tartakovsky (2009), Probabilistic risk analysis of groundwater remediation strategies, *Water Resour. Res.*, *45*, W06413, doi:10.1029/2008WR007551.
Boso, F., A. Bellin, and M. Dumbser (2013), Numerical simulations of solute transport in highly heterogeneous formations: A comparison of alternative numerical schemes, *Adv. Water Res.*, *52*, 178–189.
Bouwer, E. J., B. E. Rittmann, and P. L. McCarty (1981), Anaerobic degradation of halogenated 1- and 2-carbon organic compounds, *Environ. Sci. Technol.*, *15*(5), 596–599.
Burnell, D. K., J. W. Mercer, and C. R. Faust (2014), Stochastic modeling analysis of sequential first-order degradation reactions and non-Fickian transport in steady state plumes, *Water Resour. Res.*, *50*, 1260–1287, doi:10.1002/2013WR013814.
Clement, T. P. (1997), A modular computer code for simulating reactive multispecies transport in 3-Dimensional groundwater systems, RT3D, version 1.0, *Tech. Rep. PNNL-SA-11720*, Pac. Northwest Natl. Lab., Richland, Wash.
Clement, T. P. (2001), Generalized solution to multispecies transport equations coupled with a first-order reaction network, *Water Resour. Res.*, *37*, 157–163. .
Cui, Z., C. Welty, and R. M. Maxwell (2014), Modeling nitrogen transport and transformation in aquifers using a particle-tracking approach, *Comput. Geosci.*, *70*, 114.
Cunningham, J. A., and Z. J. Fadel (2007), Contaminant degradation in physically and chemically heterogeneous aquifers, *J. Contam. Hydrol.*, *94*(34), 293–304.
Cvetkovic, V., and R. Haggerty (2002), Transport with multiple-rate exchange in disordered media, *Phys. Rev. E*, *65*, 051308.
de Barros, F. P. J., D. Fernàndez-Garcia, D. Bolster, and X. Sanchez-Vila (2013), A risk-based probabilistic framework to estimate the endpoint of remediation: Concentration rebound by rate-limited mass transfer, *Water Resour. Res.*, *49*, 1929–1942, doi:10.1002/wrcr.20171.
Delay, F., and J. Bodin (2001), Time domain random walk method to simulate transport by advection-dispersion and matrix diffusion in fracture networks, *Geophys. Res. Lett.*, *28*, 4051–4054, doi:10.1029/2001GL013698.
Dentz, M., and A. Castro (2009), Effective transport dynamics in porous media with heterogeneous retardation properties, *Geophys. Res. Lett.*, *36*, L03403, doi:10.1029/2008GL036846.
Dentz, M., T. Le Borgne, A. Englert, and B. Bijeljic (2011), Mixing, spreading and reaction in heterogeneous media: A brief review, *J. Contam. Hydrol.*, *120*, 1–17.
De Simoni, M., J. Carrera, X. Snchez-Vila, and A. Guadagnini (2005), A procedure for the solution of multicomponent reactive transport problems, *Water Resour. Res.*, *41*, W11410, doi:10.1029/2005WR004056.
Edery, Y., H. Scher, and B. Berkowitz (2009), Modeling bimolecular reactions and transport in porous media, *Geophys. Res. Lett.*, *36*, L02407, doi:10.1029/2008GL036381.
Edery, Y., H. Scher, and B. Berkowitz (2010), Particle tracking model of bimolecular reactive transport in porous media, *Water Resour. Res.*, *46*, W07524, doi:10.1029/2009WR009017.
Fennell, D. E., A. B. Carroll, J. M. Gossett, S. H. Zinder (2001), Assessment of indigenous reductive dechlorinating potential at a TCE-contaminated site using microcosms, polymerase chain reaction analysis, and site data, *Environ. Sci. Technol.*, *35*(9), 1830–1839.
Fernàndez-Garcia, D., and X. Sanchez-Vila (2011), Optimal reconstruction of concentrations, gradients and reaction rates from particle distributions, *J. Contam. Hydrol.*, *120–121*, 99–114.
Fernàndez-Garcia, D., T. H. Illangasekare, and H. Rajaram (2004), Conservative and sorptive forced-gradient and uniform flow tracer tests in a three-dimensional laboratory test aquifer, *Water Resour. Res.*, *40*, W10103, doi:10.1029/2004WR003112.
Fernàndez-Garcia, D., T. H. Illangasekare, and H. Rajaram (2005a), Differences in the scale-dependence of dispersivity estimated from temporal and spatial moments in chemically and physically heterogeneous porous media, *Adv. Water Res.*, *28*(7), 745–759.
Fernàndez-Garcia, D., T. H. Illangasekare, and H. Rajaram (2005b), Differences in the scale-dependence of dispersivity and retardation factors estimated from forced-gradient and uniform flow tracer tests in three-dimensional physically and chemically heterogeneous porous media, *Water Resour. Res.*, *41*, W03012, doi:10.1029/2004WR003125.
Fernàndez-Garcia, D., X. Sanchez-Vila, and A. Guadagnini (2008), Reaction rates and effective parameters in stratified aquifers, *Adv. Water Res.*, *31*, 1364–1376.
Gelhar, L. W. (1993), *Stochastic Subsurface Hydrology*, 390 pp., Prentice Hall, Upper Saddle River, N. J.
Gillespie, D. (1976), A general method for numerically simulating the stochastic time evolution of coupled chemical reactions, *J. Comput. Phys.*, *22*, 403–434.
Gomez-Hernandez, J. J., and X. Wen (1998), To be or not to be multi-Gaussian? a reflection on stochastic hydrogeology, *Adv. Water Res.*, *21*(1), 47–61.
Gouze, P., T. Le Borgne, R. Leprovost, G. Lods, T. Poidras, and P. Pezard (2008), Non-Fickian dispersion in porous media: 1. Multiscale measurements using single-well injection withdrawal tracer tests, *Water Resour. Res.*, *44,W06426*, doi:10.1029/2007WR006278.
Haggerty, R., S. A. McKenna, and L. C. Meigs (2000), On the late-time behaviour of tracer test breakthrough curves, *Water Resour. Res.*, *36*, 3467–3479.
Harbaugh, A., E. Banta, M. Hill, and M. McDonald (2000), MODFLOW 2000 the US Geological Survey Modular ground-water model-user guide to modularization concepts and the ground-water flow process, *U.S. Geol. Surv. Open File Rep.*, *00-92*, 121 pp.
Haston, Z. C., and P. L. McCarty (1999), Chlorinated ethene half-velocity coefficients (Ks) for Reductive dehalogenation, *Environ. Sci. Technol.*, *33*, 223–226.
Hoehn, E., J. Eikenberg, T. Fierz, W. Drost, and E. Reichlmayr (1998), The Grimsel migration experiment: Field injection-withdrawal experiments in fractured rock with sorbing tracers, *J. Contam. Hydrol.*, *34*, 85–106.
Huang, H., A. E. Hassan, and B. X. Hu (2003), Monte Carlo study of conservative transport in heterogeneous dual-porosity media, *J. Hydrol.*, *275*, 229–241.
Jain, M. K., and C. S. Criddle (1995), Metabolism and cometabolism of halogenated C-1 and C-2 hydrocarbon, in *Biotransformations: Microbial Degradation of Health Risk Compounds*, edited by V. P. Singh, pp. 65112, Elsevier Sci., N. Y.

Kinzelbach, W. (1987), The random walk method in pollutant transport simulation, in *Advances in Analytical and Numerical Groundwater Flow and Quality Modelling, NATO ASI Ser. C*, vol. 224, edited by E. Custodio et al., pp. 227–246, Reidel, Boston, Mass.
Kitanidis, P. K. (1988), Prediction by the mothod of moments of transport in a heterogeneous formation, *J. Hydrol.*, *102*, 453–473.
Kitanidis, P. K. (1994), Particle tracking equations for the solution of the advection-dispersion equation with variable coefficients, *Water Resour. Res.*, *30*, 3225–3227.
Kräutle, S., and P. Knabner (2005), A new numerical reduction scheme for fully coupled multicomponent transport-reaction problems in porous media, *Water Resour. Res.*, *41*, W09414, doi:10.1029/2004WR003624.
Kurtz, T. G. (2003), The relationship between stochastic and deterministic models for chemical reactions, *J Chem. Phys.*, *57*(7), 2976–2978.
LaBolle, E. M., G. E. Fogg, and A. F. B. Tompson (1996), Random-walk simulation of transport in heterogeneous porous media: Local mass-conservation problem and implementation methods, *Water Resour. Res.*, *32*, 583–593.
Lawler, G. F. (2006), *Introduction to Stochastic Processes*, 234 pp., Chapman and Hall, London, U. K.
MacDonald, J. A. (2000), Evaluating natural attenuation for groundwater cleanup, *Environ. Sci. Technol.*, *34*(15), 346–353.
Maxwell, R. M., and W. E. Kastenberg (1999), Stochastic environmental risk analysis: An integrated methodology for predicting cancer risk from contaminated groundwater, *Stochastic Environ. Res. Risk Assess.*, *13*(1-2), 27–47, doi:10.1007/s004770050030.
Maxwell, R. M., S. F. Carle, and A. F. B. Tompson (2007), Contamination, risk, and heterogeneity: On the effectiveness of aquifer remediation. *Environ. Geol.*, *54*(8), 1771–1786, doi:10.1007/s00254-007-0955-8.
McCarty, P. L., and L. Semprini (1994), Ground-water treatment for chlorinated solvents, in *Handbook of Bioremediation*, edited by R. D. Norris et al., A. F. Lewis, N. Y.
Michalak, A. M., and P. K. Kitanidis (2000), Macroscopic behavior and random-walk particle tracking of kinetically sorbing solutes, *Water Resour. Res.*, *36*, 2133–2146.
Miralles-Wilhelm, F., and L. W. Gelhar (1996), Stochastic analysis of sorption macrokinetics in heterogeneous aquifers, *Water Resour. Res.*, *32*, 1541–1549, doi:10.1029/96WR00791.
Miralles-Wilhelm, F., L. W. Gelhar, and V. Kapoor (1997), Stochastic analysis of oxygen-limited biodegradation in three-dimensionally heterogeneous aquifers, *Water Resour. Res.*, *33*, 1251–1263.
Mishra, B. K., and C. Mishra (1991), Kinetics of nitrification and nitrate reduction during leaching of ammonium nitrate through a limed Ultisol profile, *J. Indian Soc. Soil Sci.*, *39*, 221–228.
Moler, C., and C. van Loan (2003), Nineteen dubious ways to compute the exponential of a matrix, twenty-five years later, *SIAM Rev.*, *45*(1), 3–49.
Molins, S., J. Carrera, C. Ayora, and M. W. Saaltink (2004), A formulation for decoupling components in reactive transport problems, *Water Resour. Res.*, *40*, W10301, doi:10.1029/2003WR002970.
Painter, S., V. Cvetkovic, J. Mancillas, and O. Pensado (2008), Time domain particle tracking methods for simulating transport with retention and first-order transformation, *Water Resour. Res.*, *44*, W01406, doi:10.1029/2007WR005944.
Palanichamy, J., T. Becker, M. Spiller, J. Kngeter, and S. Mohan (2007), Multicomponent reaction modelling using a stochastic algorithm, *Comput. Visual. Sci.*, *12*, 51–61, doi:10.1007/s00791-007-0080-y.
Paster, A., D. Bolster, and D. Benson (2014), Connecting the dots: Semi-analytical and random walk numerical solutions of the diffusion-reaction equation with stochastic initial conditions, *J. Comput. Phys.*, *263*, 91–112.
Pedretti, D., and D. Fernàndez-Garcia (2013), An automatic locally-adaptive method to estimate heavily-tailed breakthrough curves from particle distributions, *Adv. Water Res.*, *59*, 52–65.
Pedretti, D., D. Fernàndez-Garcia, D. Bolster, and X. Sanchez-Vila (2013), On the formation of breakthrough curves tailing during convergent flow tracer tests in three-dimensional heterogeneous aquifers, *Water Resour. Res.*, *49*, 4157–4173, doi:10.1002/wrcr.20330.
Rajaram, H. (1997), Time and scale dependent effective retardation factors in heterogeneous aquifers, *Adv. Water Resour.*, *20*(4), 217–230.
Rajaram, H., and L. W. Gelhar (1993), Plume scale-dependent dispersion in heterogeneous aquifers: 2. Eulerian analysis and three-dimensional aquifers, *Water Resour. Res.*, *29*, 3261–3276.
Rehfeldt, K. R., J. Mark Boggs, and L. W. Gelhar (1992), Field study of dispersion in a heterogeneous aquifer 3. Geostatistical analysis of hydraulic conductivity, *Water Resour. Res.*, *28*, 3309–3324.
Riva, M., A. Guadagnini, D. Fernandez-Garcia, X. Sanchez-Vila, and T. Ptak (2008), Relative importance of geostatistical and transport models in describing heavily tailed breakthrough curves at the Lauswiesen site, *J. Contam. Hydrol.*, *101*, 1–13.
Rubin, Y. (2003), *Applied Stochastic Hydrogeology*, Oxford Univ. Press, Oxford, U. K.
Saaltink, M. W., F. Batlle, C. Ayora, J. Carrera, and S. Olivella (2004), RETRASO, a code for modeling reactive transport in saturated and unsaturated porous media, *Geol. Acta*, *2*(3), 235–251.
Salamon, P., D. Feràndez-Garcia, J. J. Gómez-Hernández (2006a), A review and numerical assessment of the random walk particle tracking 756 method, *J. Contam. Hydrol.*, *87*, 277–305.
Salamon, P., D. Fernàndez-Garcia, and J. J. Gómez-Hernández (2006b), Modeling mass transfer processes using random walk particle tracking, *Water Resour. Res.*, *42*, W11417, doi:10.1029/2006WR004927.
Salamon, P., D. Fernàndez-Garcia, and J. J Gomez-Hernandez (2007), Modeling tracer transport at the made site: The importance of heterogeneity, *Water Resour. Res.*, *43*, W08404, doi:10.1029/2006WR005522.
Sanchez-Vila, X., J. Carrera, and J. Girardi (1996), Scale effects in transmissivity, *J Hydrol.*, *183*(1), 1–22.
Sanchez-Vila, X., D. Fernàndez-Garcia, and A. Guadagnini (2010), Interpretation of column experiments of transport of solutes undergoing an irreversible bimolecular reaction using a continuum approximation, *Water Resour. Res.*, *46*, W12510, doi:10.1029/2010WR009539.
Sandrin, S. K., M. L. Brusseau, J. J. Piatt, A. A. Boudour, W. J. Blanford, and N. T. Nelson (2004), Spatial variability of in situ microbial activity: Biotracer tests, *Ground Water*, *42*(3), 374–383.
Skeen, R. S., J. Gao, and B. S. Hooker (1995), Kinetics of chlorinated ethylene dehalogenation under methanogenic conditions, *Biotechnol. Bioeng.*, *48*, 659–666.
Smith, B. T., J. M. Boyle, J. J. Dongarra, B. S. Garbow, Y. Ikebe, V. C. Klema, and C. B. Moler (1976), *Matrix Eigensystem Routines: EISPACK Guide, Lecture Notes Comput. Sci.*, vol. 6, 551 pp., 2nd ed., Springer, N. Y.
Soga, K., J. Page, and T. Illangasekare (2004), A review of NAPL source zone remediation efficiency and the mass flux approach, *J. Hazard. Mater.*, *110*(1-3), 13–27.
Stroo, H. F., et al. (2012), Chlorinated ethene source remediation: Lessons learned, *Environ. Sci. Technol.*, *46*, 6438–6447, doi:10.1021/es204714w.
Sun, Y., J. N. Petersen, T. P. Clement, and R. S. Skeen (1999), Development of analytical solutions for multispecies transport with serial and parallel reactions, *Water Resour. Res.*, *35*, 185–190.
Tamir, A. (1998), *Applications of Markov Chains in Chemical Engineering*, 604 pp., Elsevier, Amsterdam, Netherlands.

Tompson, A. F. B. (1993), Numerical simulation of chemical migration in physically and chemically heterogeneous porous media, *Water Resour. Res.*, *29*, 3709–3726.
Tompson A. F. B, and L. W. Gelhar (1990), Numerical simulation of solute transport in three-dimensional, randomly heterogeneous porous media, *Water Resour Res*, *26*, 2541–62.
Tompson, A. F. B., A. L. Schafer, and R. W. Smith (1996), Impacts of physical and chemical heterogeneity on contaminant transport in sandy porous medium, *Water Resour. Res.*, *32* 801–818.
Tompson, A. F. B., C. J. Bruton, G. A. Pawloski, D. K. Smith, W. L. Bourcier, D. E. Shumaker, A. B. Kersting, S. F. Carle and R. M. Maxwell (2002), On the evaluation of groundwater contamination from underground nuclear tests, *Environ. Geol.*, *42*(2-3), 235–247, doi:10.1007/s00254-001-0493-8.
Trinchero, P., X. Sanchez-Vila, and D. Fernàndez-Garcia (2008), Point-to- point connectivity, an abstract concept or a key issue for risk assessment studies?, *Adv. Water Res.*, *31*, 1742–1753.
Tsang, Y. W., and C. F. Tsang (2001), A particle-tracking method for advective transport in fractures with diffusion into finite matrix blocks, *Water Resour. Res.*, *37*, 831–835.
United States Environmental Protection Agency (1998), Technical protocol for evaluating natural attenuation of chlorinated solvents in ground water, EPA/600/R-98/128, Office of Research and Development, Washington, D. C.
Valocchi, A., and H. A. M. Quinodoz (1989), Application of the random walk method to simulate the transport of kinetically adsorbing solutes, *Groundwater Contam.*, *185*, 35–42.
van Genuchten, M. T. (1985), Convective-dispersive transport of solutes involved in sequential first-order decay reactions, *Comput. Geosci.*, *11*(2), 129–147.
Vishwanathan, H. S., B. A. Robinson, A. J. Valocchi, and I. R. Triay (1998), A reactive transport model of Neptunian migration from a potential repository at Yucca Mountain, *J. Hydrol.*, *209*, 251–280.
Vogel, T. M., C. S. Criddle, and P. L. McCarty (1987), Transformations of halogenated aliphatic compounds, *Environ. Sci. Technol.*, *21*(8), 722–736.
Wen, X. H., and J. J. Gómez-Hernández (1996), The constant displacement scheme for tracking particles in heterogeneous aquifers, *Ground Water*, *34*(1), 135–142.
Willmann, M., G. W. Lanyon, P. Marschall, and W. Kinzelbach (2013), A new stochastic particle-tracking approach for fractured sedimentary formations, *Water Resour. Res.*, *49*, 352–359, doi:10.1029/2012WR012191.
Zhang, Y., and D. A. Benson (2008), Lagrangian simulation of multidimensional anomalous transport at the MADE site, *Geophys. Res. Lett.*, *35*, L07403, doi:10.1029/2008GL033222.